Article

snRNA-seq reveals a subpopulation of adipocytes that regulates thermogenesis

https://doi.org/10.1038/s41586-020-2856-x

Received: 28 December 2019

Accepted: 31 July 2020

Published online: 28 October 2020

Check for updates

Wenfei Sun[1]✉, Hua Dong[1], Miroslav Balaz[1], Michal Slyper[2], Eugene Drokhlyansky[2], Georgia Colleluori[3], Antonio Giordano[3], Zuzana Kovanicova[4], Patrik Stefanicka[5], Lucia Balazova[1], Lianggong Ding[1], Anna Sofie Husted[6], Gottfried Rudofsky[7], Jozef Ukropec[4], Saverio Cinti[3], Thue W. Schwartz[6], Aviv Regev[8,9,10] & Christian Wolfrum[1]✉

Adipose tissue is usually classified on the basis of its function as white, brown or beige (brite)[1]. It is an important regulator of systemic metabolism, as shown by the fact that dysfunctional adipose tissue in obesity leads to a variety of secondary metabolic complications[2,3]. In addition, adipose tissue functions as a signalling hub that regulates systemic metabolism through paracrine and endocrine signals[4]. Here we use single-nucleus RNA-sequencing (snRNA-seq) analysis in mice and humans to characterize adipocyte heterogeneity. We identify a rare subpopulation of adipocytes in mice that increases in abundance at higher temperatures, and we show that this subpopulation regulates the activity of neighbouring adipocytes through acetate-mediated modulation of their thermogenic capacity. Human adipose tissue contains higher numbers of cells of this subpopulation, which could explain the lower thermogenic activity of human compared to mouse adipose tissue and suggests that targeting this pathway could be used to restore thermogenic activity.

As one of the major endocrine tissues, the adipose organ is organized into different depots and can be classified as either brown adipose tissue (BAT) or white adipose tissue (WAT). It comprises approximately 20–30% mature adipocytes[5,6], as well as the stromal vascular fraction (SVF), which includes different cell types[7]. Adipocytes in turn are categorized into three different cell types: white adipocytes store energy, whereas brown adipocytes, and a related, less thermogenically efficient population referred to as beige or brite adipocytes, dissipate energy through non-shivering thermogenesis. The thermogenic ability of brown and beige (brite) adipocytes is enabled by the presence of uncoupling protein 1 (UCP1) in mitochondria[8]. In rodents, classical brown adipocytes are located within distinct areas, whereas beige or brite cells arise in response to cold stimulation within various WAT depots[7]. Previous studies have identified four distinct subtypes of in-vitro-differentiated human adipocyte clones, which are differentially associated with thermogenesis and/or lipid storage[9], as well as brown adipocytes in mice that exhibit different thermogenic activities[10,11].

Subpopulations of adipocytes in mice and humans

To comprehensively characterize mature subpopulations of brown adipocytes, we performed single-nucleus RNA sequencing (snRNA-seq)[12,13] in interscapular BAT (iBAT) from transgenic mice that express nuclear red fluorescent protein (RFP) under the control of the *Adipoq* promoter (Extended Data Fig. 1a, Methods). Using RFP as a selection feature, we profiled 377 high-quality nuclei by snRNA-seq[14] (Extended Data Fig. 1b, Methods), and detected 1,999 genes, on average. Unsupervised clustering identified three adipocyte subpopulations—clusters C1, C2 and C3 (Extended Data Fig. 1b, Methods). Canonical adipocyte markers and brown adipocyte markers[15] were expressed in all groups (Extended Data Fig. 1c), albeit at varying levels. Preadipocyte markers (*Ly6a* and *Cd34*; Extended Data Fig. 1c) were found in cluster C2, indicating that these could be differentiating precursor cells[16,17]. Trajectory analysis suggested that these cells differentiate from population C2 to C1 (Extended Data Fig. 1d, e). C3 cells (15 out of 377 cells; Extended Data Fig. 1b) represent a distinct population of brown adipocytes with expression of specific marker genes, including *Cyp2e1* (Extended Data Fig. 1c, f, Supplementary Table 1). We validated the grouping by profiling an additional 8,827 adipocyte nuclei by snRNA-seq using the 10X Genomics Chromium system[18] (Extended Data Fig. 1g–k, Supplementary Table 2, Methods). Brown adipocytes partitioned into four populations that we name P-RT-1–P-RT-4 (in which RT refers to room temperature, 21–23 °C) (Extended Data Fig. 1g, h). Most nuclei expressed brown-adipocyte-specific markers (Extended Data Fig. 1i), whereas markers of preadipocytes (Extended Data Fig. 1j) or stromal cells were virtually absent (Extended Data Fig. 1k, data not shown). Besides *Cyp2e1*, P-RT-4 cells (256 out of 8,827 cells; Extended Data Fig. 1g) expressed similar markers to C3 (Extended Data Fig. 1i).

To examine the dynamics of iBAT, we profiled 6,560 adipocyte nuclei from mice that were kept at 30 °C for 120 days (thermoneutrality) (Extended Data Fig. 1l–o, Supplementary Table 3) and 11,074 adipocyte nuclei from mice that were kept at 8 °C for 4 days (cold-exposure

[1]Institute of Food, Nutrition and Health, ETH Zurich, Schwerzenbach, Switzerland. [2]Broad Institute of MIT and Harvard, Cambridge, MA, USA. [3]Department of Experimental and Clinical Medicine, Center of Obesity, Marche Polytechnic University, Ancona, Italy. [4]Institute of Experimental Endocrinology, Biomedical Research Center at the Slovak Academy of Sciences, Bratislava, Slovakia. [5]Department of Otorhinolaryngology–Head and Neck Surgery, Faculty of Medicine and University Hospital, Comenius University, Bratislava, Slovakia. [6]The Novo Nordisk Foundation Center for Basic Metabolic Research, University of Copenhagen, Copenhagen, Denmark. [7]Department of Endocrinology, Cantonal Hospital Olten, Olten, Switzerland. [8]Klarman Cell Observatory, Broad Institute of MIT and Harvard, Cambridge, MA, USA. [9]Howard Hughes Medical Institute, Koch Institute of Integrative Cancer Research, Department of Biology, Massachusetts Institute of Technology, Cambridge, MA, USA. [10]Present address: Genentech, South San Francisco, CA, USA. ✉e-mail: wenfei-sun@ethz.ch; christian-wolfrum@ethz.ch

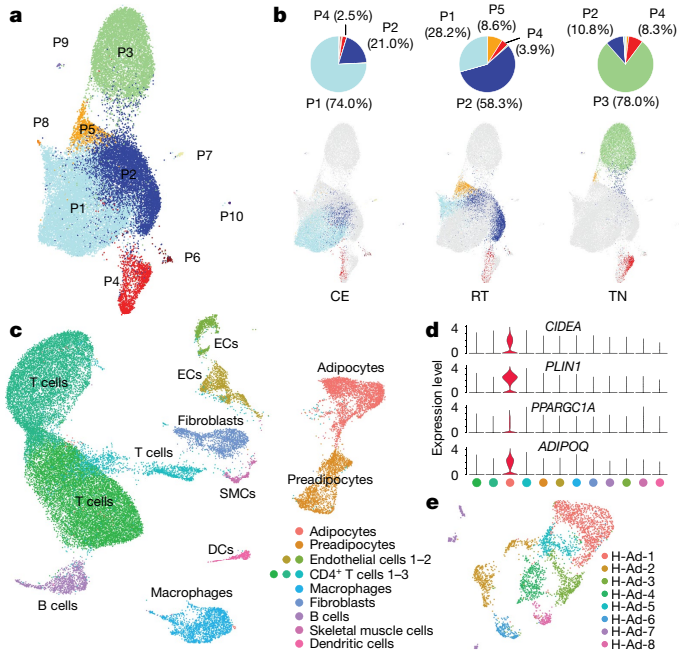

Fig. 1 | Identification of adipocyte populations in BAT. a, **b**, Integrated analysis of snRNA-seq including 28,771 adipocyte nuclei from iBAT in thermoneutral, room-temperature and cold-exposure conditions, yielding 1,265 genes (median). The ten subpopulations (P1–P10) are shown. **a**, Unsupervised clustering shown as uniform manifold approximation and projection (UMAP) plots. **b**, Cluster compositions in different conditions (CE, cold exposure; RT, room temperature; TN, thermoneutral). **c**–**e**, snRNA-seq of human deep-neck BAT. **c**, Unsupervised clustering of 36,590 nuclei from human BAT, yielding 1,975 (median) genes. DC, dendritic cells; EC, endothelial cells; SMCs, skeletal muscle cells. **d**, Violin plots for *CIDEA*, *PPARGC1A*, *PLIN1* and *ADIPOQ*. Expression level (*y* axis) refers to the log normalized ratio of gene-expression reads, normalized to the sum of all reads within each nucleus. **e**, Unsupervised subclustering of 3,607 adipocyte nuclei from human BAT, yielding 1,253 (median) genes. The eight subpopulations of human adipocytes (H-Ad-1–H-Ad-8) are shown.

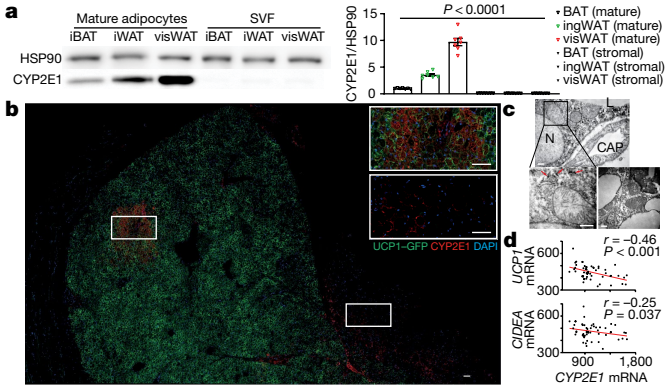

Fig. 2 | A distinct population of adipocytes is present in mouse iBAT and ingWAT and in human deep-neck BAT. a, Blot (left) and quantification (right) of the levels of CYP2E1 protein in mature adipocytes and SVF of three adipose tissue depots (iBAT, iWAT and visWAT). $n = 7$ mice, $F = 167.3$, degrees of freedom (df) = 41. **b**, Immunofluorescence staining of CYP2E1 in iBAT of Ucp1-GFP mice at room temperature. Representative image from six independent experiments. Scale bars, 50 µm. **c**, Electron microscopy analysis of CYP2E1 staining in mouse iBAT. Red arrows indicate CYP2E1$^+$ cells. Top, CYP2E1$^+$ positive adipocyte; bottom, CYP2E1$^-$ adipocyte. CAP, capillary; L, lipid droplets; N, nuclei. Scale bars, 200 nm. **d**, Correlation of the relative levels of *CYP2E1* mRNA with the levels of *UCP1* and *CIDEA* mRNA in human WAT. $n = 52$ individuals. Data are mean average ± s.e.m. Statistical significance was calculated using a one-way analysis of variance (ANOVA) (**a**) or Pearson's correlation coefficient (**d**).

conditions) (Extended Data Figs. 1p, q, 2a, Supplementary Table 4). An integrated analysis of nuclei from mice kept under each of the three conditions (room temperature, cold exposure or thermoneutrality) revealed ten subpopulations (Fig. 1a, Supplementary Table 5), with P1 and P2 derived mainly from the room-temperature and cold-exposure groups, P3 mainly from the thermoneutral group, P5 from the room-temperature group and P6–P10 mainly from the cold-exposure group (Extended Data Fig. 2b, Fig. 1b). P4 contained nuclei from all three conditions (at a frequency of 2.5%, 3.9% and 8.3% for cold exposure, room temperature and thermoneutrality, respectively; Fig. 1b). Trajectory analysis identified three main states of cells that correspond to the three temperature conditions, whereas P4 cells were in the early stage of each progression (Extended Data Fig. 2c).

We next tested whether a similar population of adipocytes is present in human BAT. Unsupervised clustering of 36,590 nuclei from 16 individuals identified 12 subsets[19] (Fig. 1c, d, Extended Data Figs. 2m, 3a–d, Supplementary Table 6, Methods). A Garnett classifier trained with ADIPOQ$^+$ cells as a reference identified an additional 510 adipocytes outside the main adipocyte cluster (Extended Data Fig. 3c). To stratify the adipocyte population, we performed subclustering, which identified 8 subpopulations within the predicted 3,607 adipocytes (Fig. 1e, Extended Data Fig. 3e–g, Supplementary Table 7). In contrast to mice, several subpopulations of human adipocytes were positive for P4 markers. To expand these data, we analysed 2,438 nuclei from subcutaneous WAT from 5 individuals (Extended Data Fig. 3h–l, Supplementary Table 8, Methods). The P4 gene signature (Extended Data Fig. 3a, f, j) showed a greater enrichment in the nuclei of brown adipocytes than white adipocytes, indicating that there is a higher proportion of P4 cells in human BAT than WAT.

Localization of CYP2E1$^+$ adipocytes

To further characterize P4 cells, we analysed the expression of the most prominent marker gene, *Cyp2e1*, which was restricted to the mature adipocyte fraction in BAT and WAT[20] (Fig. 2a). To assess the localization of CYP2E1 expression, we performed immunostaining in iBAT and the adjacent subscapular WAT (subscWAT) of Ucp1-GFP mice[6]. We found that a distinct CYP2E1$^+$ population of unilocular, paucilocular and multilocular cells (Fig. 2b) was localized both at the edge of and within iBAT (Extended Data Fig. 4a). Quantification revealed that approximately 10% of all adipocytes within iBAT and 20% within subscWAT expressed CYP2E1 (Extended Data Fig. 4b). An analysis comparing the expression of P4 marker genes (*Aldh1a1*, *Nrip1*, *Auts2*, *Atp2b4*, *Cyp2e1* and so on) with bulk RNA expression data from iBAT, subscWAT and inguinal WAT (ingWAT) did not reveal any overlap with any of the three depots, indicating that these P4 cells cannot be classified according to existing categories (Extended Data Fig. 4c–e). In accordance with our single-nucleus data, we observed that the number of CYP2E1$^+$ cells decreased after cold exposure and increased under thermoneutral conditions (Extended Data Fig. 4f–i). It has been suggested that BAT in mice expands by recruiting new brown adipocytes at the edges of the depot[21]. P4 cells might therefore be newly formed brown adipocytes (Extended Data Fig. 2c). However, this is at odds with our observation that the population is increased under the thermoneutral condition, which would reduce the recruitment of new brown adipocytes.

To perform a more detailed analysis of P4 cells, we acquired electron microscopy images of mouse iBAT immunostained for CYP2E1 (Fig. 2c). CYP2E1$^+$ cells exhibited an ultrastructure analagous to that of brown adipocytes, but their mitochondria were smaller and contained randomly oriented cristae similar to structures that have been previously described[22]. An analysis of other adipose tissue depots showed that there was a higher percentage of CYP2E1$^+$ P4 cells in ingWAT compared

to iBAT both at room temperature and after cold exposure. At room temperature, CYP2E1$^+$ cells were mainly unilocular (Extended Data Fig. 4j), whereas in cold-exposure conditions we observed both multilocular and unilocular cells (Extended Data Fig. 4k); by contrast, in visceral WAT (visWAT) CYP2E1$^+$ cells were exclusively unilocular (Extended Data Fig. 4l).

In human adipose tissue from the deep-neck region, both multilocular and unilocular cells stained positive for CYP2E1, suggesting that these cells constitute a subpopulation that can acquire different morphologies (Extended Data Fig. 4n–p). The prominent P4 signature observed in human brown adipocytes, and the high abundance of P4 markers within more than one subpopulation of human adipocytes, suggest that the prevalent human adipocyte is similar to an adipocyte from the mouse P4 subgroup. This might be explained by the fact that humans spend a substantial amount of their time under conditions that are close to thermoneutrality[23]. Given the aberrant mitochondrial structure that was observed in CYP2E1$^+$ cells, as well as their localization within the mature adipocyte fraction, we analysed samples of adipose tissue samples from obese and overweight individuals, who have lower adipocyte thermogenic activity[24]. Notably, *CYP2E1* mRNA expression was inversely correlated—albeit weakly—with the expression of *UCP1* and *CIDEA* (Fig. 2d).

CYP2E1$^+$ adipocytes control thermogenesis

As alterations in the structure of mitochondria are likely to compromise their function, we examined whether mouse P4 cells are associated with changes in BAT activity (Supplementary Table 5). One gene that is coexpressed exclusively with *Cyp2e1* is *Aldh1a1* (encoding aldehyde dehydrogenase 1 family member A1), which has been implicated in adipose tissue thermogenesis[25]. Co-staining of both markers in mouse iBAT (Fig. 3a, Extended Data Fig. 5a) showed a complete overlap, demonstrating that of the mature adipocytes in iBAT, ingWAT and visWAT, only P4 brown adipocytes express ALDH1A1 (Extended Data Fig. 5b), independent of UCP1 expression (Extended Data Fig. 5c). Furthermore, we observed an increase in the expression of ALDH1A1 under thermoneutral conditions, whereas ALDH1A1 protein and mRNA levels were slightly reduced after cold exposure (Extended Data Fig. 5d, e). To test whether P4 constitutes a subpopulation with altered thermogenic function, we generated a GFP-expressing adeno-associated virus (AAV) that expresses a short hairpin RNA (shRNA) to knock down *Aldh1a1* specifically in mature adipocytes (Extended Data Fig. 5f, g). The specificity of the system was tested using AdipoCre-NucRed transgenic mice, which were analysed under room-temperature, cold-exposure and thermoneutral conditions (Fig. 3b). We observed efficient knockdown of *Aldh1a1* in iBAT (Fig. 3c) and exclusive targeting of mature adipocytes, as evidenced by the coexpression of NucRed and GFP (Extended Data Fig. 5g). No biologically meaningful changes were seen in ALDH1A1 expression in visWAT and ingWAT (Extended Data Fig. 5h), which was expected given the specific Cre expression[26]. After cold exposure, mice with deletion of *Aldh1a1* had a significantly higher neck surface temperature (Fig. 3d) and exhibited significantly increased levels of UCP1 in iBAT (Fig. 3c, e, Extended Data Fig. 6a, b) compared to control mice. This is in line with previous reports suggesting that loss of *Aldh1a1* protects against obesity and that this protection is associated with an increase in BAT function[25,27]. The increases in UCP1 levels and in body temperature were less pronounced under thermoneutral conditions (Extended Data Fig. 7a–c) and mice in which *Aldh1a1* expression was knocked down selectively in iBAT showed a higher uptake of glucose in iBAT both in room-temperature and in cold-exposure conditions (Fig. 3f, Extended Data Fig. 7g). Furthermore, deletion of *Aldh1a1* in iBAT led to a higher oxygen consumption (Extended Data Fig. 7h), which was more pronounced after cold exposure. This effect was independent of any changes in UCP1 expression in ingWAT (Extended Data Fig. 7d–f), suggesting that the observed phenotype was due to changes

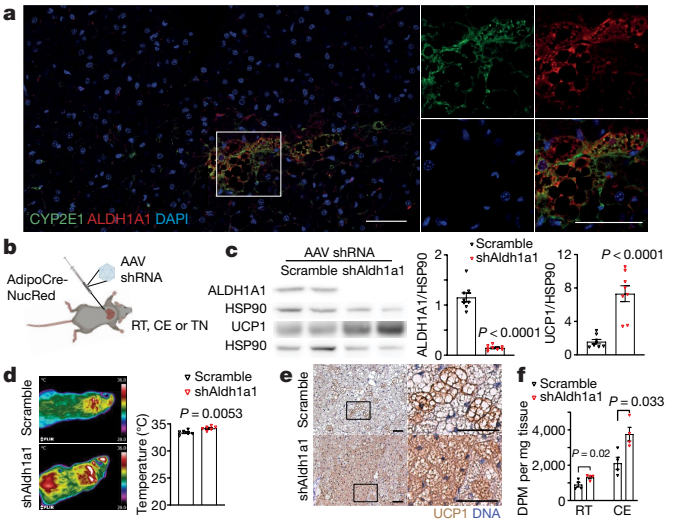

Fig. 3 | Reduction of ALDH1A1 expression in mature adipocytes of iBAT promotes thermogenesis and whole-body energy expenditure in mice. **a**, Co-staining of CYP2E1 and ALDH1A1 in iBAT at room temperature. Representative image from five independent experiments. Scale bars, 50 µm. **b**, Schematic illustration of the experimental set-up. AdipoCre-NucRed mice were analysed under room-temperature (9 weeks), cold-exposure (4 days) or thermoneutral (9 weeks) conditions. **c**, ALDH1A1 and UCP1 protein levels in iBAT after AAV-shRNA-mediated knockdown of *Aldh1a1*. $n = 8$ mice, $t_{ALDH1A1} = 11.10$, $t_{UCP1} = 5.82$, df = 14. **d**, Surface temperature of AAV-injected mice after four days of cold exposure. $n = 6$ mice, $t = 3.55$, df = 10. **e**, Immunohistochemical staining of UCP1 in iBAT from AAV-injected mice after cold exposure. Representative image from four independent experiments. Scale bars, 50 µm. **f**, Glucose uptake in iBAT of AAV-injected mice at room temperature or after four days of cold exposure. DPM, disintegrations per minute. $n = 4$ mice, $t_{RT} = 2.74$, $t_{CE} = 3.19$, df = 6. Data are mean average ± s.e.m. Statistical significance was calculated using a two-tailed unpaired Student's *t*-test (**c**, **d**, **f**).

in iBAT thermogenic capacity. To mimic the thermoneutral condition, we injected an AAV that overexpresses *Aldh1a1* into iBAT in mice and studied the physiological changes (Extended Data Fig. 7i). We were able to achieve a twofold induction of expression, similar to the increase in the thermoneutral versus the room-temperature condition (Extended Data Fig. 7j). We observed a slight decrease in the levels of UCP1 in iBAT, as well as reduced energy expenditure and neck surface temperature (Extended Data Fig. 7j–l), confirming that ALDH1A1 levels control the thermogenic properties of the tissue. In light of the small percentage of P4 cells in iBAT (around 2.9%), this finding suggests either that P4 cells become the main contributors to systemic energy expenditure after the loss of *Aldh1a1*, or that these cells interact with other cells to modulate whole-organ thermogenesis.

Acetate signalling and BAT function

To study the thermogenic capacity of P4 cells in more detail, we differentiated the SVF from iBAT and ingWAT in a dish and—in accordance with the in vivo data—observed a heterogeneous mixture of differentiated adipocytes, with approximately 17% of iBAT-derived and 23% of ingWAT-derived adipocytes expressing both ALDH1A1 and CYP2E1 (Fig. 4a, Extended Data Fig. 8a, b). These data suggest that P4 cells might arise from committed precursors, in line with the idea that the heterogeneity of the adipocyte precursor pool determines the heterogeneity of mature adipocytes[28]. Expression of both CYP2E1 and ALDH1A1 was induced upon adipocyte development (Extended Data Fig. 8c, d) and, moreover, we observed that most of the ALDH1A1$^+$ cells were UCP1$^-$, independent of the mitochondrial content (Extended Data Fig. 8e, f).

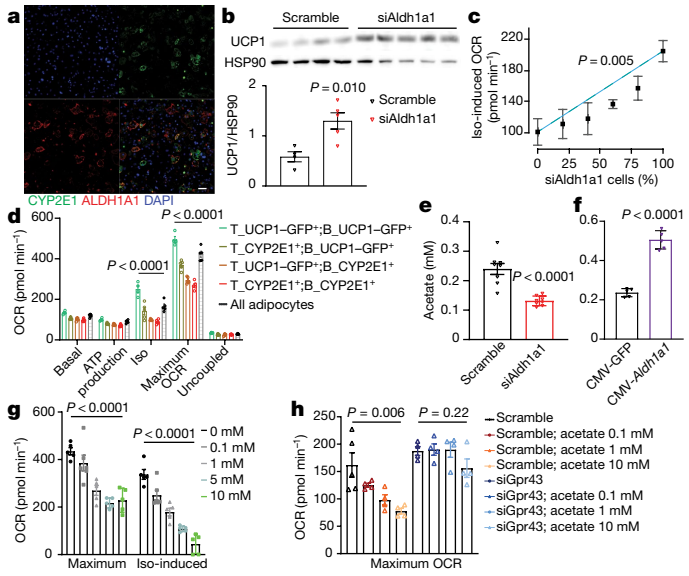

Fig. 4 | ALDH1A1 regulates brown adipocyte thermogenic capacity through acetate. a, Immunofluorescence staining of ALDH1A1 and CYP2E1 in differentiated brown adipocytes from iBAT. Representative image from five independent experiments. Scale bar, 50 µm. **b**, UCP1 expression after siRNA-mediated knockdown of *Aldh1a1* in brown adipocytes. $n = 4$ (scramble), $n = 5$ (siAldh1a1), $t = 3.51$, df = 7. **c**, Isoproterenol (iso)-induced oxygen consumption rate (OCR) in brown adipocytes. Cells transfected with scramble siRNA or siRNA targeting *Aldh1a1* were mixed at different ratios. $n = 4$, $t_{60\%} = 7.35$, df = 3. **d**, OCR of FACS-selected and co-cultured cells. Uncoupled refers to uncoupled respiration. $n = 5$ (except $n = 4$ for the T_UCP1–GFP$^+$;B_UCP1–GFP$^+$ cohort (in which T and B refer to top and bottom, respectively)), $F_{iso} = 27.83$, $F_{max} = 60.62$. **e**, Levels of acetate in the culture medium of mature adipocytes after *Aldh1a1* knockdown. $n = 8$, $t = 5.58$, df = 14. **f**, Levels of acetate in the culture medium of mature adipocytes after *Aldh1a1* overexpression using a cytomegalovirus (CMV) promoter. $n = 5$, $t = 6.47$, df = 8. **g**, OCR in brown adipocytes treated with the indicated levels of acetate during differentiation days 4–8. $n = 5$ (except $n = 6$ for the 0.1 mM cohort), $F_{max} = 17.88$, $F_{iso} = 41.56$. **h**, OCR in brown adipocytes treated with the indicated levels of acetate with or without *Gpr43* knockdown. $n = 4$ (except $n = 5$ for the scramble cohort), $F_{scramble} = 6.71$, $F_{siGpr43} = 1.70$. Data are mean average ± s.e.m. n represents the number of independent experiments. Statistical significance was calculated using a two-tailed unpaired t-test (**b**, **e**, **f**), one sample t-test (**c**) or one-way ANOVA (**d**, **g**, **h**).

To modulate the function of these cells, we reduced the expression of *Aldh1a1* using short interfering RNA (siRNA) (Extended Data Fig. 8g), which did not affect adipogenesis or cell numbers (Extended Data Fig. 8h). Ablation of *Aldh1a1* led to an increase in UCP1 expression (Fig. 4b) and an induction of other brown-adipocyte-specific genes (Extended Data Fig. 8i), owing to an increased number of UCP1$^+$ cells (Extended Data Fig. 8h). The data were corroborated by a respirometry analysis of adipocytes that were differentiated from iBAT ex vivo and in which *Aldh1a1* expression was ablated; these adipocytes showed an increase in their consumption of oxygen (Extended Data Fig. 8j), reminiscent of an increase in the function of brown adipocytes.

Given the increased number of UCP1$^+$ cells, the increase in the levels of UCP1 and the induction of respiratory capacity after reduction of ALDH1A1 in only 17% of the differentiated cells, we speculated that the effect was due to a paracrine interaction between P4 cells and other thermogenic cells. To test this hypothesis, we differentiated SVF cells with cells that were treated with *Aldh1a1* siRNA[29] or scrambled siRNA, mixed at different ratios. We observed an *Aldh1a1*-siRNA dose-dependent increase in oxygen consumption that was substantially less pronounced than the expected linear increase (Fig. 4c, Extended Data Fig. 8k), suggesting that P4 cells modulate the thermogenic activity of other cells. To support this hypothesis, we performed co-culture experiments in a transwell system to exclude the regulation of activity by cell contacts (Extended Data Fig. 8l). Elimination of *Aldh1a1* in the bottom chamber alone led to a mild increase of *Ucp1* expression and respiration, whereas ablation in both chambers had a similar effect to that of *Aldh1a1* ablation in the complete culture (Extended Data Fig. 8m, n). To substantiate these findings, we differentiated brown adipocytes from iBAT of Ucp1-GFP mice and separated the cells into CYP2E1$^+$ and UCP1–GFP$^+$ cells by fluorescence-activated cell sorting (FACS) at an early stage of differentiation (Extended Data Fig. 9a, b). We found that *Aldh1a1* was enriched in CYP2E1$^+$ cells, whereas the expression of *Ucp1* was reduced and *Pparg* expression remained unchanged (Extended Data Fig. 9c). When these cells were cultivated in a transwell system, we observed the highest levels of *Ucp1* expression and oxygen consumption when UCP1–GFP$^+$ cells were cultured in both chambers, and the lowest levels of *Ucp1* expression and oxygen consumption when CYP2E1$^+$ cells were cultured in both chambers (Fig. 4d, Extended Data Fig. 9d, e). To address the question of whether an increase in ALDH1A1 expression would cause the opposite phenotype, we infected cells with a lentivirus that overexpresses *Aldh1a1*. Infection led to a fivefold overexpression of *Aldh1a1* and a reduction in the number of UCP1$^+$ cells, as well as a reduction in *Ucp1* mRNA levels and a decrease in respiration (Extended Data Fig. 9f–j). Together, these data demonstrate that ALDH1A1$^+$CYP2E1$^+$ cells express a paracrine factor that represses the thermogenic capacity of brown adipocytes.

Loss of *Aldh1a1* has been shown to lead to an increase in the levels of retinaldehyde, which activates brown adipocyte function[25,27,30]. We therefore quantified retinaldehyde levels after knockdown of *Aldh1a1* expression and found that loss of *Aldh1a1* led to a twofold increase in retinaldehyde, close to the detection limit, in both the extracellular and the intracellular compartment (Extended Data Fig. 9k, l). Treatment of brown adipocytes with varying amounts of different retinoids showed, as reported previously[31–33], that retinoic acid—a possible product of retinaldehyde conversion by ALDH1A1—was as efficacious in modulating brown adipocyte thermogenic capacity as retinaldehyde (Extended Data Fig. 9m). The addition of retinaldehyde in the range of the observed concentrations was not sufficient to alter brown adipocyte thermogenesis (Extended Data Fig. 9n).

As ALDH1A1 has been reported to produce acetate from acetaldehyde[34–36], we quantified acetate levels in the supernatant of cells in which *Aldh1a1* expression was modulated. We observed a twofold decrease in acetate levels after *Aldh1a1* knockdown, and a twofold increase when ALDH1A1 expression was induced (Fig. 4e, f). Similarly, acetate levels increased by twofold in total iBAT in thermoneutral conditions (Extended Data Fig. 9o). Brown adipocytes express high levels of hydroxymethylglutaryl (HMG)-CoA synthase 2[37], the rate-limiting enzyme of ketone body synthesis, in addition to D-β-hydroxybutyrate dehydrogenase (BDH1)[24], which is required for the conversion of acetoacetate to generate β-hydroxybutyrate. Thus, it is possible that acetoacetate is converted into acetaldehyde, which might be metabolized by ALDH1A1 to form acetate. To test whether acetate influences the function of brown adipocytes, we titrated brown adipocytes with acetate during differentiation and measured cellular respiration and UCP1 expression. We observed a dose-dependent decrease in the number of UCP1$^+$ cells (Extended Data Fig. 9p), in the levels of *Ucp1* mRNA (Extended Data Fig. 10a) and in isoproterenol-induced respiration in both mouse and human brown adipocytes (Fig. 4g, Extended Data Fig. 10b, c). To test whether the effect of *Aldh1a1* ablation could be rescued by the addition of acetate, we treated mouse brown adipocytes in which *Aldh1a1* expression was ablated with varying levels of acetate. In line with our findings, we observed that the effects of *Aldh1a1* deletion could be blocked by the addition of acetate at physiological levels (Extended Data Fig. 10d). As we could demonstrate the regulation of thermogenic capacity in a paracrine manner, we next

tested whether the effect was caused by extracellular or intracellular acetate. As shown in Extended Data Fig. 10e, f, we did not observe any rescue of the phenotype when acetate transporters were blocked, suggesting that extracellular acetate levels are more relevant. Given that G-protein-coupled receptor 43 (GPR43) has been described as an autocrine and paracrine cell-surface sensor of acetate in β-cells that is expressed in adipocytes[38], we tested whether part of the effect was mediated by this receptor. We ablated the expression of *Gpr43* by siRNA knockdown, which led to an increase in the levels of *Ucp1* mRNA (Extended Data Fig. 10g). Furthermore, we observed that cells with reduced expression of *Gpr43* were less responsive to acetate (Fig. 4h, Extended Data Fig. 10h), whereas a synthetic GPR43 agonist was able to inhibit the rate of oxygen consumption in mouse adipocytes to a similar degree to acetate (Extended Data Fig. 10i, j).

Although acetate has been implicated in many physiological processes, the data are conflicting with regard to the role of acetate in obesity[39]. This might be due to the fact that acetate can be produced by the gut microbiome; however, it is expected that acetate is not completely removed by the liver, which would result in the integration of an acetate signal from systemic and paracrine sources that ultimately controls thermogenic capacity. In line with this hypothesis, a previous cross-sectional study found that circulating—but not fecal—acetate is negatively correlated with whole-body lipolysis and insulin sensitivity[40].

Owing to the complexity of the analysis, our study has several limitations. First, the single-cell analysis was done in adult mice only; we therefore cannot deduce whether we identified a distinct type of adipocyte, or whether P4 cells represent adipocytes in a different state (similar to P3 cells, which consist of adipocytes with altered gene expression at thermoneutrality). Second, although we observed an increase in respiration and metabolic flux after ablation of *Aldh1a1* in iBAT, we cannot link these changes to systemic metabolic changes, owing to the lack of model systems. The same problem applies to the human context, and therefore in-depth analyses using longitudinal cohorts will be required. Finally, we focused on ALDH1A1; nevertheless, it might be possible that other functional genes in P4 adipocytes influence the function of adipose tissue.

In conclusion, we provide here an in-depth single-cell analysis of mature brown and white adipocytes in both mice and humans. The $CYP2E1^{+}ALDH1A1^{+}$ population of cells that we have identified controls the thermogenic function of other adipocytes in a paracrine manner by modulating the levels of the short-chain fatty acid acetate. This mechanism is likely to have evolved to preserve energy under thermoneutral conditions, and might be leveraged to modulate the thermogenic capacity of adipose tissue.

Online content

Any methods, additional references, Nature Research reporting summaries, source data, extended data, supplementary information, acknowledgements, peer review information; details of author contributions and competing interests; and statements of data and code availability are available at https://doi.org/10.1038/s41586-020-2856-x.

1. Cannon, B. & Nedergaard, J. Brown adipose tissue: function and physiological significance. *Physiol. Rev.* **84**, 277–359 (2004).
2. Lauby-Secretan, B. et al. Body fatness and cancer—viewpoint of the IARC working group. *N. Engl. J. Med.* **375**, 794–798 (2016).
3. Hajer, G. R., van Haeften, T. W. & Visseren, F. L. J. Adipose tissue dysfunction in obesity, diabetes, and vascular diseases. *Eur. Heart J.* **29**, 2959–2971 (2008).
4. Scheele, C. & Wolfrum, C. Brown adipose cross talk in tissue plasticity and human metabolism. *Endocr. Rev.* **41**, 53–65 (2019).
5. Roh, H. C. et al. Warming induces significant reprogramming of beige, but not brown, adipocyte cellular identity. *Cell Metab.* **27**, 1121–1137 (2018).
6. Rosenwald, M., Perdikari, A., Rülicke, T. & Wolfrum, C. Bi-directional interconversion of brite and white adipocytes. *Nat. Cell Biol.* **15**, 659–667 (2013).
7. Rosenwald, M. & Wolfrum, C. The origin and definition of brite versus white and classical brown adipocytes. *Adipocyte* **3**, 4–9 (2014).
8. Jung, S. M., Sanchez-Gurmaches, J. & Guertin, D. A. in *Brown Adipose Tissue. Handbook of Experimental Pharmacology* Vol. 251 3–36 (2018).
9. Min, S. Y. et al. Diverse repertoire of human adipocyte subtypes develops from transcriptionally distinct mesenchymal progenitor cells. *Proc. Natl Acad. Sci. USA* **116**, 17970–17979 (2019).
10. Song, A. et al. Low- and high-thermogenic brown adipocyte subpopulations coexist in murine adipose tissue. *J. Clin. Invest.* **130**, 247–257 (2020).
11. Rajbhandari, P. et al. Single cell analysis reveals immune cell-adipocyte crosstalk regulating the transcription of thermogenic adipocytes. *eLife* **8**, e49501 (2019).
12. Habib, N. et al. Massively parallel single-nucleus RNA-seq with DroNc-seq. *Nat. Methods* **14**, 955–958 (2017).
13. Habib, N. et al. Div-Seq: single-nucleus RNA-seq reveals dynamics of rare adult newborn neurons. *Science* **353**, 925–928 (2016).
14. Picelli, S. et al. Full-length RNA-seq from single cells using Smart-seq2. *Nat. Protocols* **9**, 171–181 (2014).
15. Shinoda, K. et al. Genetic and functional characterization of clonally derived adult human brown adipocytes. *Nat. Med.* **21**, 389–394 (2015).
16. Schwalie, P. C. et al. A stromal cell population that inhibits adipogenesis in mammalian fat depots. *Nature* **559**, 103–108 (2018).
17. Merrick, D. et al. Identification of a mesenchymal progenitor cell hierarchy in adipose tissue. *Science* **364**, eaav2501 (2019).
18. Gaublomme, J. T. et al. Nuclei multiplexing with barcoded antibodies for single-nucleus genomics. *Nat. Commun.* **10**, 2907 (2019).
19. Aran, D. et al. Reference-based analysis of lung single-cell sequencing reveals a transitional profibrotic macrophage. *Nat. Immunol.* **20**, 163–172 (2019).
20. Sebastian, B. M. et al. Identification of a cytochrome P4502E1/Bid/C1q-dependent axis mediating inflammation in adipose tissue after chronic ethanol feeding to mice. *J. Biol. Chem.* **286**, 35989–35997 (2011).
21. Lee, Y.-H., Petkova, A. P., Konkar, A. A. & Granneman, J. G. Cellular origins of cold-induced brown adipocytes in adult mice. *FASEB J.* **29**, 286–299 (2015).
22. Cinti, S. *Obesity, Type 2 Diabetes and the Adipose Organ* (Springer, 2018).
23. Keijer, J., Li, M. & Speakman, J. R. What is the best housing temperature to translate mouse experiments to humans? *Mol. Metab.* **25**, 168–176 (2019).
24. Perdikari, A. et al. BATLAS: deconvoluting brown adipose tissue. *Cell Rep.* **25**, 784–797 (2018).
25. Kiefer, F. W. et al. Retinaldehyde dehydrogenase 1 regulates a thermogenic program in white adipose tissue. *Nat. Med.* **18**, 918–925 (2012).
26. Eguchi, J. et al. Transcriptional control of adipose lipid handling by IRF4. *Cell Metab.* **13**, 249–259 (2011).
27. Ziouzenkova, O. et al. Retinaldehyde represses adipogenesis and diet-induced obesity. *Nat. Med.* **13**, 695–702 (2007).
28. Wu, J. et al. Beige adipocytes are a distinct type of thermogenic fat cell in mouse and human. *Cell* **150**, 366–376 (2012).
29. Yang, K. et al. Aldehyde dehydrogenase 1 a1 regulates energy metabolism in adipocytes from different species. *Xenotransplantation* **24**, e12318 (2017).
30. Yasmeen, R. et al. Autocrine function of aldehyde dehydrogenase 1 as a determinant of diet- and sex-specific differences in visceral adiposity. *Diabetes* **62**, 124–136 (2013).
31. Alvarez, R. et al. A novel regulatory pathway of brown fat thermogenesis. Retinoic acid is a transcriptional activator of the mitochondrial uncoupling protein gene. *J. Biol. Chem.* **270**, 5666–5673 (1995).
32. Matthias, A. et al. Thermogenic responses in brown fat cells are fully UCP1-dependent. *J. Biol. Chem.* **275**, 25073–25081 (2000).
33. Tourniaire, F. et al. All-trans retinoic acid induces oxidative phosphorylation and mitochondria biogenesis in adipocytes. *J. Lipid Res.* **56**, 1100–1109 (2015).
34. Li, H., Toth, E. & Cherrington, N. J. Alcohol metabolism in the progression of human nonalcoholic steatohepatitis. *Toxicol. Sci.* **164**, 428–438 (2018).
35. Mews, P. et al. Alcohol metabolism contributes to brain histone acetylation. *Nature* **574**, 717–721 (2019).
36. Liu, X. et al. Acetate production from glucose and coupling to mitochondrial metabolism in mammals. *Cell* **175**, 502–513 (2018).
37. Balaz, M. et al. Inhibition of mevalonate pathway prevents adipocyte browning in mice and men by affecting protein prenylation. *Cell Metab.* **29**, 901–916 (2019).
38. Husted, A. S., Trauelsen, M., Rudenko, O., Hjorth, S. A. & Schwartz, T. W. GPCR-mediated signaling of metabolites. *Cell Metab.* **25**, 777–796 (2017).
39. Hernández, M. A. G., Canfora, E. E., Jocken, J. W. E. & Blaak, E. E. The short-chain fatty acid acetate in body weight control and insulin sensitivity. *Nutrients* **11**, 1943 (2019).
40. Müller, M. et al. Circulating but not faecal short-chain fatty acids are related to insulin sensitivity, lipolysis and GLP-1 concentrations in humans. *Sci. Rep.* **9**, 12515 (2019).

Methods

Data reporting

No statistical methods were used to predetermine sample size. The experiments were not randomized and the investigators were not blinded to allocation during experiments and outcome assessment.

Clinical sample acquisition

The clinical study was approved by the local ethics committee of the University Hospital in Bratislava, Slovakia. All study participants provided witnessed written informed consent before entering the study. Samples of BAT were obtained from the lower third of the neck by an experienced ear, nose and throat surgeon during neck surgery under general anaesthesia. The deep-neck BAT samples were taken from the pre- and paravertebral space between the common carotid and trachea in the case of thyroid surgery and just laterally to the carotid sheath in the case of branchial cleft cyst surgery. Subcutaneous WAT samples were taken from underneath the skin. In all cases, the surgical approach was sufficient to reach and sample the deep-neck adipose tissue without any additional morbidity. Patients with malignant disease and individuals younger than 18 years were excluded from participation in the study. Deep-neck BAT samples were collected from 16 individuals (4 male and 12 female; 49.2 ± 19.0 years (22–77 years); BMI 24.8 ± 4.7 kg/m^2 (16.9–35.2 kg/m^2); body fat 29.1 ± 8.5% (15.6–46.6%); thyroid surgery, $n = 14$ or branchial cleft cyst surgery, $n = 2$; data are expressed as mean average ± s.d.). Samples were cleaned immediately from blood and connective tissue, frozen in liquid nitrogen and stored at −80 °C until isolation of nuclei.

Isolation of nuclei from human tissue

Nuclei were isolated following a modified nuclear isolation protocol[41]. In brief, frozen human BAT tissues were thawed on ice, minced to 1 mm^3 and homogenized in cold 0.1% CHAPS in Tris-HCl. The minced adipose tissue was filtered through a 40-µm cell strainer and centrifuged at 500*g* for 5 min at 4 °C, and the pellet was resuspended in phosphate-buffered saline (PBS) with DAPI. Nuclei suspensions were loaded to a MoFlo Astrios EQ Cell Sorter and sorted into a 1.5-ml tube.

Mice

Wild-type C57BL/6 N mice were obtained from Charles River Laboratories. Unless indicated otherwise, all experiments were performed with adult male mice that were kept on an inverted 12-h:12-h dark:light cycle and fed ad libitum with a chow diet, at 40% humidity. For cold stimulation, mice were housed in long type-II cages at 8 °C. For thermoneutral condition, mice were housed in long type-II cages at 30 °C. All animal studies were approved by the Veterinäramt Zürich.

Isolation of nuclei from mouse tissue

iBAT was collected from seven-week-old AdipoCre-NucRed transgenic mice (B6.FVB-Tg(Adipoq-cre)1Evdr/J x B6;129-Gt(ROSA)$^{26Sortm7(CAG-tdTomato*)Nat}$/J) for each experiment. Nuclei were isolated by following a modified DroNc-seq protocol[12]. Tissue was minced to 1 mm^3, homogenized in Nuclei EZ Lysis Buffer (NUC101, Sigma-Aldrich) on ice and filtered through a 40-µm cell strainer. This was followed by centrifugation at 500*g* for 5 min at 4 °C and the pellet was resuspended in PBS. Resuspended nuclei were loaded to a MoFlo Astrios EQ Cell Sorter and RFP$^+$ nuclei were collected individually in a 384-well plate for Smart-seq2 or 10X sequencing.

snRNA-seq

Smart-seq2-based libraries[42] were generated following a modified Div-Seq method[13]. In brief, sorted individual nuclei were reverse-transcribed with oligo-dT, TSO, Super Scriptase II, reverse transcription (RT) buffer, dNTP, betaine, $MgCl_2$ and RNase inhibitor. Then the RT product was amplified by 21 PCR cycles with ISPCR primer and the KAPA HiFi kit and then purified with AMPure XP beads. The PCR products were fragmented using the Nextera XT kit and sequenced on a NextSeq 500 (Illumina). Primer sequences are available upon request. 10X-based libraries were generated following the manufacturer's protocol. In brief, a suspension of 1,000 nuclei per µl was loaded to 10X chromium with a v3 kit. Sequencing was performed using a NovaSeq (Illumina). Sequencing data were analysed following a protocol based on the Seurat[43] package v3.1.1 and Monocle v2.14.0 (ref. [44]) on R 3.6.1 (ref. [45]).

10X-based libraries were acquired with the Chromium Single Cell V3.0 reagent kit following the manufacturer's protocol (10X Genomics). Nuclei suspensions containing around 500 nuclei per µl were loaded into nine independent lanes. Libraries were sequenced on a NovaSeq 6000 (Illumina). For data analysis, first we applied CellBender[46] to distinguish cell-containing droplets from empty droplets; Then we applied Scrublet[47] and DoubletFinder[48] to exclude potential doublets, and nuclei that expressed both male and female signature genes were excluded from downstream analysis. The human genome assembly GRCh38.p13 and mouse genome assembly GRCm38.p5 were used for mapping. CCA[49] from the Seurat package was used for batch correcting, clustering and identification of signature genes. SingleR[19] was used to annotate cell clusters.

AAV production

AAV plasmids were ordered from VectorBuilder, with an shRNA sequence targeting *Aldh1a1* (CCGCAATGAAGATATCTCAGAATAGTGAAGCCACAGATGTATTCTGAGATATCTTCATTGCGA) or scrambled control. The AAV for the overexpression of *Aldha1a* was produced by inserting the *Aldh1a1* coding sequence or GFP under the control of the *Ucp1* mini promoter. Ten micrograms of targeting vector was co-transfected with 40 µg pDP8 and 200 µl PEI (1 mg ml^{-1}) in a passage 15 (P15) of 293AAV cells (AAV-100, Cell Biolabs), at 40% confluence. The culture medium was refreshed 24 h after transfection. The culture medium was collected 72 h after transfection and concentrated using the AAVanced Concentration Reagent (AAV100A-1, System Biosciences). Schematic illustration (Fig. 3b) created with BioRender.com.

AAV administration

AAV injection was performed following an established protocol[50]. AdipoCre-NucRed mice were anaesthetized with isoflurane. A longitudinal incision was made in the interscapular region to expose the brown fat depot, and six injections with 10 µl of AAV (10^{13} vg/ml) were distributed into both sides of brown fat.

Lentivirus production

A lentiviral construct was produced by inserting the *Aldh1a1* coding sequence or GFP under the control of the CMV promoter into pLenti-MP2 (plasmid 36097). See scheme in Extended Data Fig. 9f. Ten micrograms of targeting vector was co-transfected with 3 µg pDM2.G, 8 µg of psPAX2 and 84 µl PEI (1 mg ml^{-1}) into a P10 dish of 293LTV cells (LTV-100, Cell Biolabs), at 70% confluence. The culture medium was refreshed 16 h after transfection. The culture medium was collected 72 h after transfection and concentrated with PEG-it Virus Precipitation Solution (LV810A-1, System Biosciences). TransDux MAX Lentivirus Transduction Reagent (LV860A-1, System Biosciences) was applied for transducing lentivirus particles into primary adipocytes.

Isolation and culture of primary adipocytes

For SVF isolation, dissected adipose tissues were minced with scissors and incubated in 1 mg ml^{-1} collagenase (C6885-1G, Sigma-Aldrich) in collagenase buffer (25 mM $NaHCO_3$, 12 mM KH_2PO_4, 1.2 mM $MgSO_4$, 4.8 mM KCl, 120 mM NaCl, 1.4 mM $CaCl_2$, 5 mM glucose, 2.5% BSA, 1% penicillin–streptomycin, pH = 7.4) for 50 min at 37 °C under agitation. An equal volume of culture medium (high-glucose DMEM medium (61965026, Gibco) supplemented with 10% FBS and 1% penicillin–streptomycin)

was added and samples were centrifuged for 5 min at 300*g*. The SVF pellet was resuspended in 2 ml erythrocyte lysis buffer (154 mM NH_4Cl, 10 mM $KHCO_3$, 0.1 mM EDTA, pH 7.4) and incubated for 4 min at room temperature. Samples were diluted with 10 ml culture medium and filtered through 40-µm cell strainers. After 5 min of centrifugation at 300*g*, the supernatant was removed, and the pellets were resuspended in culture medium. SVF cells were seeded into a plate precoated with collagen I (1:500, C3867, Sigma-Aldrich) and differentiated as described previously[51]. Forty-eight hours after differentiation induction, cells were cultured with maintenance cocktail (1 µM rosiglitazone and 0.12 µg ml^{-1} insulin) and refreshed every 48 h. To test the effects of acetate on brown adipocyte function, the culture medium was supplemented with different amounts of acetate during differentiation. To quantify acetate, primary brown adipocytes on differentiation day 8 were washed three times with PBS, and incubated with maintenance cocktail for 24 h; 100 µl culture medium was collected and acetate levels were quantified using the Acetate Colorimetric Assay Kit (MAK086-1KT, SIGMA), following the manufacturer's protocol.

Co-culture experiments

On differentiation day 4, primary cells were reverse-transfected with a pool of three siRNA probes. In brief, 75,000 cells per cm^2 were seeded into transwell inserts or receiver plates with 100 nM of corresponding siRNA, which was dissolved in 1.5% Lipofectamine RNAiMAX (13778150, Invitrogen) in Opti-MEM I reduced serum medium (31985062, Invitrogen). forty-eight hours after transfection, the inserts and receiver plates were washed with warm PBS twice, and co-cultured as described in Extended Data Fig. 8l in maintenance cocktail. After four days of co-culture, cells were collected for protein extraction or reseeded in a seahorse plate at a density of 8,000 cells per well for measuring cellular respiration.

FACS of mature adipocytes

On differentiation day 7, *Ucp1*-GFP iBAT-derived cells were detached from a P10 dish by incubation with collagenase (1 mg ml^{-1}) in collagenase buffer for 30 min at 37 °C. The cell resuspension was centrifuged for 5 min at 300*g*, and the cell pellet was resuspended in 20 ml FACS buffer. The cell suspension was filtered through 100-µm cell strainers and centrifuged at 300*g* for another 5 min. After removal of the supernatant and resuspension of the cell pellet in FACS buffer to 0.5×10^7 cells per ml, cells were incubated with anti-mouse CYP2E1– allophycocyanin (APC) (1:50) for 20 min protected from light, followed by two washes with 10 ml FACS buffer. Anti-CYP2E1 antibody (Thermo Fisher Scientific PA5-35351) was conjugated with APC (Expedeon SKU705-0030), following the manufacturer's instructions. After the final wash, the cell pellet was resuspended in FACS buffer to a concentration of 1×10^6 cells per ml. Samples were loaded onto a Sony SH800 cell sorter (100-µm chip), and the target populations were gated as shown in Extended Data Fig. 9a. Target populations were collected with culture medium, then seeded in a 96-well seahorse culture plate with co-culture inserts for functional analysis (see 'Co-culture experiments'). The extracellular respiration experiment was performed after four days of co-culture.

Extracellular respiration measurement with acetate transporter inhibitor

BAT-derived SVF cells were differentiated to day 6, and AR-C155858 (1 µM), SR13800 (1 µM), α-cyano-4-hydroxycinnamic acid (1 mM), carbonyl cyanide m-chlorophenyl hydrazone (1 µM), monensin (1 mM) or mercury chloride (10 µM) were added to cells. Afterwards sodium acetate (1 mM, pH adjusted to 7.3) was added to cells. The medium with compounds and acetate was refreshed daily for three days until OCR measurements.

Retinaldehyde quantification

Retinaldehyde levels were quantified by high-performance liquid chromatography (HPLC) as described previously[52]. In brief, mouse brown adipocyte cell culture medium or cell lysate samples were collected as described above and spiked with defined concentrations of retinaldehyde using a standard addition methodology. Retinaldehyde was subsequently converted to the oxime derivate, extracted by hexane and then quantified on a standard curve using an IFC-UltiMate-3000 HPLC system and a Zorbax SB-C18, 4.6 × 100-mm, 3.5-µm column with UV-based detection at 368 nM, as previously described[52].

siRNA knockdown titration experiment

On differentiation day 3, primary BAT-derived cells were reverse-transfected with corresponding siRNA (Supplementary Table 9) following the protocol described above ('Co-culture experiments'). Seventy-two hours after reverse transfection, primary cells were collected for protein extraction. The scramble-siRNA-transfected cells were mixed at different ratios with *Aldh1a1*-siRNA-transfected cells (ranging from 0 to 100%) at a density of 8,000 cells per well in seahorse plates for the extracellular respiration experiment.

Indirect calorimetry

Indirect calorimetry measurements were performed with the Phenomaster (TSE Systems) according to the manufacturer's guidelines and protocols. Mice were single-caged and acclimated to the metabolic cages for 48 h before metabolic recording.

Surface temperature measurement

Surface temperature was recorded with an infrared camera at room temperature (E60; FLIR) and analysed with FLIR Tools software (FLIR).

Tracing of radiolabelled glucose

Tissue radiolabelled glucose uptake was measured, as described previously[53]. Mice were fasted for 4 h, then ^{14}C-2-deoxyglucose at 8 mM, 14.8 MBq per kg body weight was injected by tail vein. Blood samples were collected 30 min after injection. Tissue was collected, weighed and lysed in 10 volumes of 0.5 M NaOH. Radioactivity was measured by liquid scintillation counting (100 µl of lysate in 3.9 ml of Emulsifier-Safe, Perkin Elmer).

Analysis of adipocyte differentiation

Differentiated adipocytes at day 8 were used for differentiation analysis. In brief, cells in a 96-well optical plate were washed with PBS twice and fixed with 5% formaldehyde at 4 °C for 10 min, followed by washing 3 times with PBS. Cells were stained with LD540 (100 ng $µl^{-1}$) for lipid droplets and Hoechst no. 33342 (100 ng $µl^{-1}$). For UCP1 staining, lipids were depleted by 5% acetic acid in ethanol for 10 min at −20 °C, washed with PBS twice at room temperature and blocked in 0.05% triton, 5% BSA and PBS. Cells were incubated with UCP1 antibody (1:500, ab10983, Abcam) overnight, washed twice in PBS and incubated with Alexa Fluor 488 anti-rabbit (1:500, A-11034, Thermo Fisher Scientific) secondary antibody and DAPI, followed by three washing steps. A total of 29 images per well were acquired with an automated microscope imaging system (Operetta, Perkin Elmer). Images were analysed using the Operetta imaging software Harmony.

Histology and image analysis

Adipose tissues were excised, fixed in fresh 4% paraformaldehyde in PBS (Gibco; pH 7.4) for 24 h at 4 °C, dehydrated and then embedded with paraffin. Paraffin sections (4 µm) were subjected to histological staining. Heat-induced antigen retrieval was applied on rehydrated paraffin sections. After blocking with 5% BSA for one hour, primary antibody (1:200 UCP1, PA1-24894, Thermo Fisher Scientific) diluted in 5% BSA was applied to sections overnight at 4 °C. After washing with PBS, a secondary antibody (Signal Stain Boost IHC, 8114, Cell Signaling Technology) was applied and the sections were washed three times and detected using the DAB method (80259P, Cell Signaling Technology). Standard haematoxylin and eosin (H&E) staining was performed on

rehydrated fat paraffin sections. Slides were dehydrated and covered with coverslips by resin-based mounting. All images were acquired by Axioscope A.1.

Fluorescence immunostaining of adipose cryosections

Adipose tissues from mice were excised and fixed in fresh 4% paraformaldehyde (Sigma-Aldrich) in PBS (Gibco) at pH 7.4 for 2 h at 4 °C, washed 4 times in PBS and cryopreserved for 30 h in 30% sucrose in PBS with stirring at 4 °C. The samples were flash-frozen on dry ice and stored at −80 °C. BAT was cut at −25 °C on an HM 500 O microtome (Microm) at 20-µm thickness, mounted on Superfrost plus slides (Medite), thawed at 4 °C and blocked with 10% donkey serum in PBS for 1 h, followed by UCP1 (ab10983, Abcam), CYP2E1 (ab28146, Abcam) and ALDH1A1 (ab9883, Abcam) antibodies overnight in 10% donkey serum in PBS. Sections were washed three times with PBS at room temperature, stained with Alexa 488 anti-rabbit (A-11034, Thermo Fisher Scientific), Alexa 594 anti-goat (A-11058, Thermo Fisher Scientific) secondary antibody and 300 nM DAPI for 1 h. Slides were embedded in ProLong Diamond Antifade Mountant (P36965, Themo Fisher Scientific). Native UCP1–GFP signal was acquired without antibody staining. Fluorescence micrographs were acquired on an SP8 confocal microscope (Leica). Background was adjusted using samples without primary antibody.

Immunoelectron microscopy

Immunoelectron microscopy was performed on fixed samples following a modified version of this protocol[54]. In brief, after overnight fixation at 4 °C, samples were reduced in small thin slices (around 1 mm × 4 mm), placed in 0.5-ml tubes and washed with phosphate buffer (0.1 M) for 5 min at room temperature; 3% H_2O_2 (in PBS; 5 min) was then used to block endogenous peroxidase and samples were rinsed with PBS. They were then incubated with the primary rabbit polyclonal anti-Cytochrome P450 2E1 antibody (1:50 v/v) in PBS overnight at 4 °C. After a thorough rinse in PBS, samples fragments were incubated for one hour in a 1:100 v/v secondary antibody (Vector Laboratories) solution at room temperature. Histochemical reactions were performed using a Vectastain ABC kit (one hour at room temperature; Vector Laboratories) and Sigma Fast 3,3′-diaminobenzidine (10 min; Sigma-Aldrich) as the substrate. Samples were then reduced in around 1 mm × 1-mm fragments and fixed again in 2% glutaraldehyde–2% paraformaldehyde in phosphate buffer overnight at 4 °C. Samples were then post-fixed in 1% osmium tetroxide, dehydrated in a graded series of acetone and embedded in an Epon-Araldite mixture. To determine the region of interest, semi-thin sections were cut and stained with toluidine blue. Thin sections were obtained with an MT-X Ultratome (RMC), stained with lead citrate and examined with a CM10 transmission electron microscope (Philips).

Extracellular respiration

Primary brown adipocytes were counted and plated at a density of 8,000 cells per well in a seahorse plate and cultured with the cocktail described above ('Isolation and culture of primary adipocytes'). At differentiation day 8, mature brown adipocytes were loaded to an XF_{96} Extracellular Flux Analyzer (Agilent). Mitochondrial respiration and the extracellular acidification rate was quantified using the Mito-stress test protocol. After measurement of basal respiration, oligomycin (1 µg ml^{-1} inhibitor of complex V) was injected to block respiration coupled to ATP synthesis. A decrease in OCR after oligomycin injection reflects the contribution of coupled respiration to the basal mitochondrial OCR. Uncoupled respiration was in the next step induced with isoproterenol (1 µM), to quantify the capacity of cells to dissipate energy through uncoupled respiration. FCCP (1 µg ml^{-1}) was injected to fully uncouple the mitochondrial membrane and to quantify the maximum respiratory capacity of brown adipocytes. In the last step, rotenone (3 µM) and antimycin A (2 µg ml^{-1}) were injected to block mitochondrial respiration (complex I and III) and estimate the contribution of non-mitochondrial respiration to the measured OCR. Non-mitochondrial respiration was subtracted to obtain basal, basal uncoupled, isoproterenol-stimulated uncoupled and maximum mitochondrial respiration[53].

Extracellular respiration in human multipotent adipose-derived stem cells

Human multipotent adipose-derived stem cells (MADS) were cultured for brown adipocyte induction as we previously described[37]. Sodium acetate was added to the culture medium from day 16, with the pH adjusted to 7.3. The medium was refreshed daily until cellular respiration was measured on day 17. All cell lines used were regularly tested for mycoplasma contamination and tested negative throughout the whole duration of the study.

Western blot

Protein samples were isolated from adipose tissue with RIPA buffer (50 mM Tris-HCl pH 7.5), 150 mM NaCl, 1 mM EDTA, 1% Triton X-100, 0.1% SDS, 10% glycerol) supplemented with protease inhibitor cocktail (11697498001, Sigma-Aldrich) and Halt Phosphatase Inhibitor (78420, Thermo Fisher Scientific). Homogenized protein lysates were obtained by rotating at 4 °C for 30 min, followed by centrifugation at 14,000 rpm for 30 min. Protein amounts were quantified using the DC Protein Assay (Bio-Rad). For immunoblotting, protein samples were separated by SDS–PAGE on 12% polyacrylamide gels and transferred onto a nitrocellulose membrane. Membranes were probed using the indicated antibodies and chemiluminescent signals was detected by a LAS 4000 mini ImageQuant system (GE Healthcare). Band intensity was quantified using ImageJ. UCP1 (ab10983, Abcam), CYP2E1 (ab28146, Abcam), ALDH1A1 (ab52492, Abcam), HSP90 (4887, Cell Signaling Technology) and HRP anti-rabbit (Calbiochem) were used.

Reporting summary

Further information on research design is available in the Nature Research Reporting Summary linked to this paper.

Data availability

All RNA sequencing (RNA-seq) data that support this finding of this study have been deposited in ArrayExpress, with the accession codes E-MTAB-8561 for snRNA-seq of mouse interscapular brown adipocytes at room temperature by Smart-seq2; E-MTAB-8562 for snRNA-seq of mouse interscapular brown adipocytes in room-temperature, cold-exposure and thermoneutral conditions by 10X sequencing; E-MTAB-8564 for snRNA-seq of human BAT cells; E-MTAB-9199 for snRNA-seq of human subcutaneous WAT cells; and E-MTAB-9192 for bulk RNA-seq of mouse iBAT, subscWAT and ingWAT. The datasets can be explored interactively at https://batnetwork.org/. Please address correspondence and requests for materials to C.W. and requests for bioinformatic information to W.S. Source data are provided with this paper.

41. Drokhlyansky, E. et al. The human and mouse enteric nervous system at single-cell resolution. *Science* **182**, 1606–1622.e23 (2020).
42. Chen, W., Gardeux, V., Meireles-Filho, A. & Deplancke, B. Profiling of single-cell transcriptomes. *Curr. Protoc. Mouse Biol.* **7**, 145–175 (2017).
43. Satija, R., Farrell, J. A., Gennert, D., Schier, A. F. & Regev, A. Spatial reconstruction of single-cell gene expression data. *Nat. Biotechnol.* **33**, 495–502 (2015).
44. Qiu, X. et al. Reversed graph embedding resolves complex single-cell trajectories. *Nat. Methods* **14**, 979–982 (2017).
45. Ihaka, R. & Gentleman, R. R: a language for data analysis and graphics. *J. Comput. Graph. Stat.* **5**, 299–314 (1996).
46. Fleming, S. J., Marioni, J. C. & Babadi, M. CellBender remove-background: a deep generative model for unsupervised removal of background noise from scRNA-seq datasets. Preprint at https://doi.org/10.1101/791699 (2019).
47. Wolock, S. L., Lopez, R. & Klein, A. M. Scrublet: computational identification of cell doublets in single-cell transcriptomic data. *Cell Syst.* **8**, 281–291 (2019).
48. McGinnis, C. S., Murrow, L. M. & Gartner, Z. J. DoubletFinder: doublet detection in single-cell RNA sequencing data using artificial nearest neighbors. *Cell Syst.* **8**, 329–337 (2019).

49. Stuart, T. et al. Comprehensive integration of single-cell data. *Cell* **177**, 1888–1902 (2019).
50. Modica, S. et al. BMP4 promotes a brown to white-like adipocyte shift. *Cell Rep*. **16**, 2243–2258 (2016).
51. Rosenwald, M., Efthymiou, V., Opitz, L. & Wolfrum, C. SRF and MKL1 independently inhibit brown adipogenesis. *PLoS One* **12**, e0170643 (2017).
52. Kane, M. A. & Napoli, J. L. Quantification of endogenous retinoids. *Methods Mol. Biol*. **652**, 1–54 (2010).
53. Sun, W. et al. Cold-induced epigenetic programming of the sperm enhances brown adipose tissue activity in the offspring. *Nat. Med*. **24**, 1372–1383 (2018).
54. Cinti, S., Cigolini, M., Morroni, M. & Zingaretti, M. C. S-100 protein in white preadipocytes: an immunoelectronmicroscopic study. *Anat. Rec*. **224**, 466–472 (1989).
55. Pliner, H. A., Shendure, J. & Trapnell, C. Supervised classification enables rapid annotation of cell atlases. *Nat. Methods* **16**, 983–986 (2019).
56. Yu, G., Wang, L.-G., Han, Y. & He, Q.-Y. clusterProfiler: an R package for comparing biological themes among gene clusters. *OMICS* **16**, 284–287 (2012).
57. Enomoto, M., Bunge, M. B. & Tsoulfas, P. A multifunctional neurotrophin with reduced affinity to p75NTR enhances transplanted Schwann cell survival and axon growth after spinal cord injury. *Exp. Neurol*. **248**, 170–182 (2013).

Acknowledgements We are grateful to R. Freimann for assistance with nuclei FACS; E. Yángüez for assistance with 10X and Smart-seq2 experiments; E. D. Rosen for discussions and suggestions; D. Peleg for discussions and suggestions on HPLC analysis; O. Ashenberg, Y. Shen, Y. He, U. Ghoshdastider, G. Tan, B. Deplancke, P. Rainer and T. Wang for comments on the bioinformatics analyses; and W. Koppenol and E. Kiehlmann for histology tissue sections. Data produced and analysed in this paper were generated in collaboration with the Functional Genomics Center Zurich, the Cytometry Facility of University of Zurich and the Scientific Center for Optical and Electron Microscopy of ETH. The work was supported by the Swiss National Science Foundation (SNSF 185011 to C.W.).

Author contributions W.S. conceived the study; W.S. and C.W. designed the study; W.S. and H.D. performed all of the experimental work except for that described below. W.S. analysed the transcriptome data with input from A.R.; W.S., H.D., M.B., Z.K. and J.U. collected BAT from patients; P.S. performed surgery for collection of human BAT; W.S., H.D., M.S. and E.D. developed the nuclei acquisition methods; C.W. and W.S. acquired retinaldehyde quantification data; L.B. acquired human MADS data; T.W.S. and A.S.H. advised and oversaw *Gpr43* work; G.C., A.G. and S.C. acquired immunoelectron microscope pictures; and G.R. acquired Optifast clinical data. C.W., W.S. and A.R. wrote the manuscript. H.D., M.B., S.C., L.D. and A.S.H. helped with editing of the manuscript.

Competing interests A.R. is a co-founder and equity holder of Celsius Therapeutics, an equity holder in Immunitas Therapeutics and a scientific advisory board member of Thermo Fisher Scientific, Syros Pharmaceuticals, Asimov and Neogene Therapeutics. As of 1 August 2020, A.R. is an employee of Genentech.

Additional information

Supplementary information is available for this paper at https://doi.org/10.1038/s41586-020-2856-x.

Correspondence and requests for materials should be addressed to W.S. or C.W.

Peer review information *Nature* thanks Patrick Seale and the other, anonymous, reviewer(s) for their contribution to the peer review of this work.

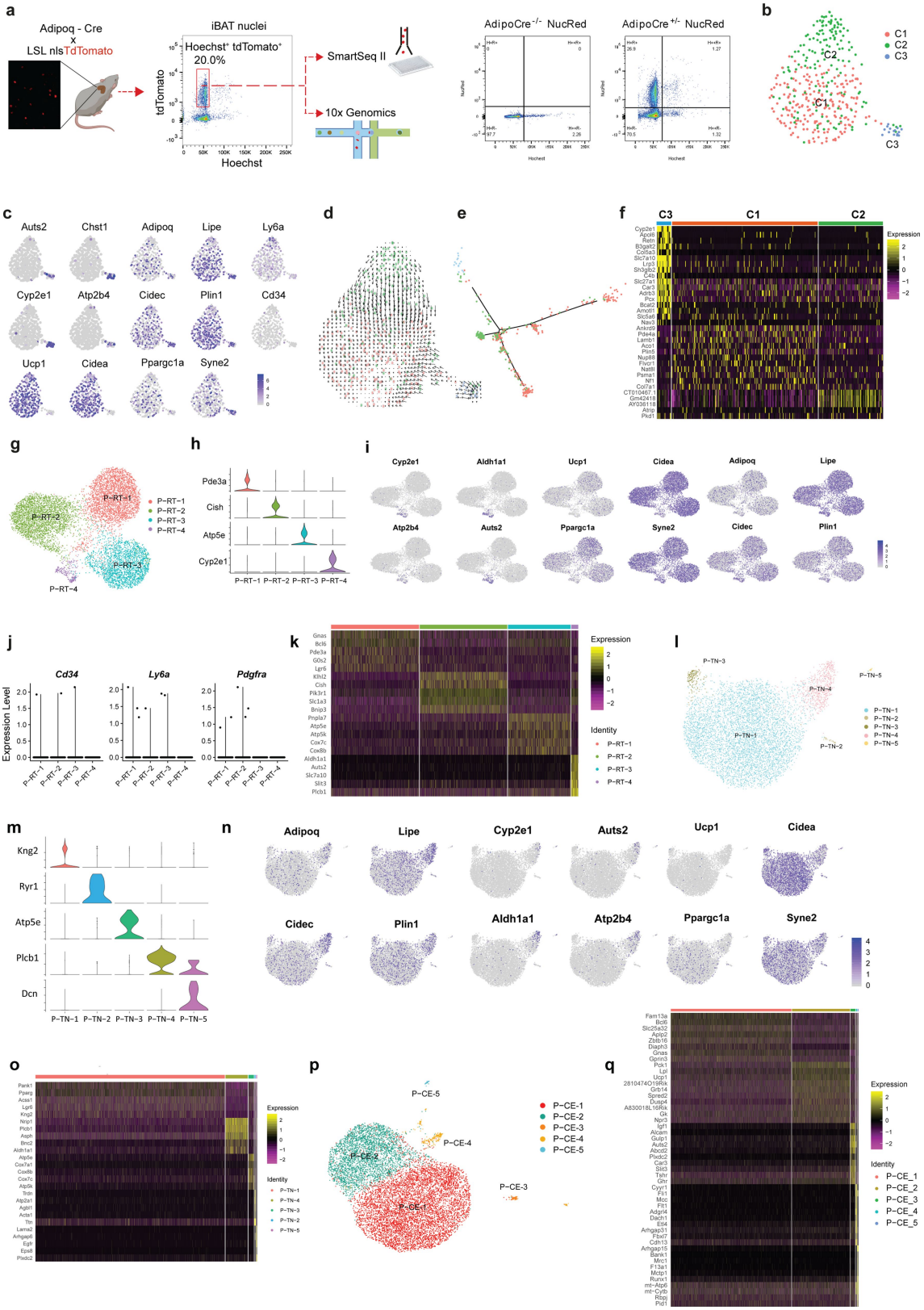

Extended Data Fig. 1 | See next page for caption.

Extended Data Fig. 1 | Identification of subpopulations of mouse brown adipocytes. a, Schematic illustration of adipocyte snRNA-seq and nuclei FACS plot of *AdipoCre*$^{-/-}$*NucRed* and *AdipoCre*$^{-/+}$*NucRed*. **b**–**f**, snRNA-seq of 377 adipocyte nuclei from iBAT at room temperature, by Smart-seq2 protocol, yielding 1,999 genes (median) detected. **b**, Unsupervised clustering shown as UMAP. **c**, Feature plots for *Auts2*, *Chst1*, *Cyp2e1*, *Atp2b4*, *Adipoq*, *Lipe*, *Cidec*, *Plin1*, *Ucp1*, *Cidea*, *Ppargc1a*, *Syne2*, *Ly6a* and *Cd34*. **d**, **e**, Trajectory analysis of brown adipocyte nuclei by RNA velocity (**d**) and by Monocle (**e**). **f**, Heat map of signature genes for each population of brown adipocyte nuclei. **g**–**k**, snRNA-seq of 8,827 adipocyte nuclei from iBAT at room temperature, by 10X protocol. **g**, Unsupervised clustering shown as UMAP. **h**, Violin plot of *Pde3a*, *Cish*, *Atp5e*, *Cyp2e1* **i**, Feature plots for *Cyp2e1*, *Atp2b4*, *Aldh1a1*, *Auts2*, *Ucp1*, *Cidea*, *Ppargc1a*, *Syne2*, *Adipoq*, *Lipe*, *Cidec* and *Plin1*. **j**, Violin plot of *Cd34*, *Ly6a* and *Pdgfra*. **k**, Heat map of signature genes for each population. **l**–**o**, snRNA-seq of 6,560 adipocytes in BAT at thermoneutrality, by 10X protocol. **l**, Unsupervised clustering shown as UMAP. **m**, Violin plot of *Kng2*, *Plcb1*, *Atp5e*, *Ryr1* and *Dcn*. **n**, Feature plots of *Adipoq*, *Lipe*, *Cidec*, *Plin1*, *Cyp2e1*, *Auts2*, *Aldh1a1*, *Atp2b4*, *Ucp1*, *Cidea*, *Ppargc1a* and *Syne2*. **o**, Heat map of signature genes for each population. **p**, **q**, snRNA-seq of 11,074 adipocytes from mouse iBAT in cold-exposure conditions. **p**, Unsupervised clustering shown as UMAP. **q**, Heat map of signature genes for each population. This figure is related to Fig. 1.

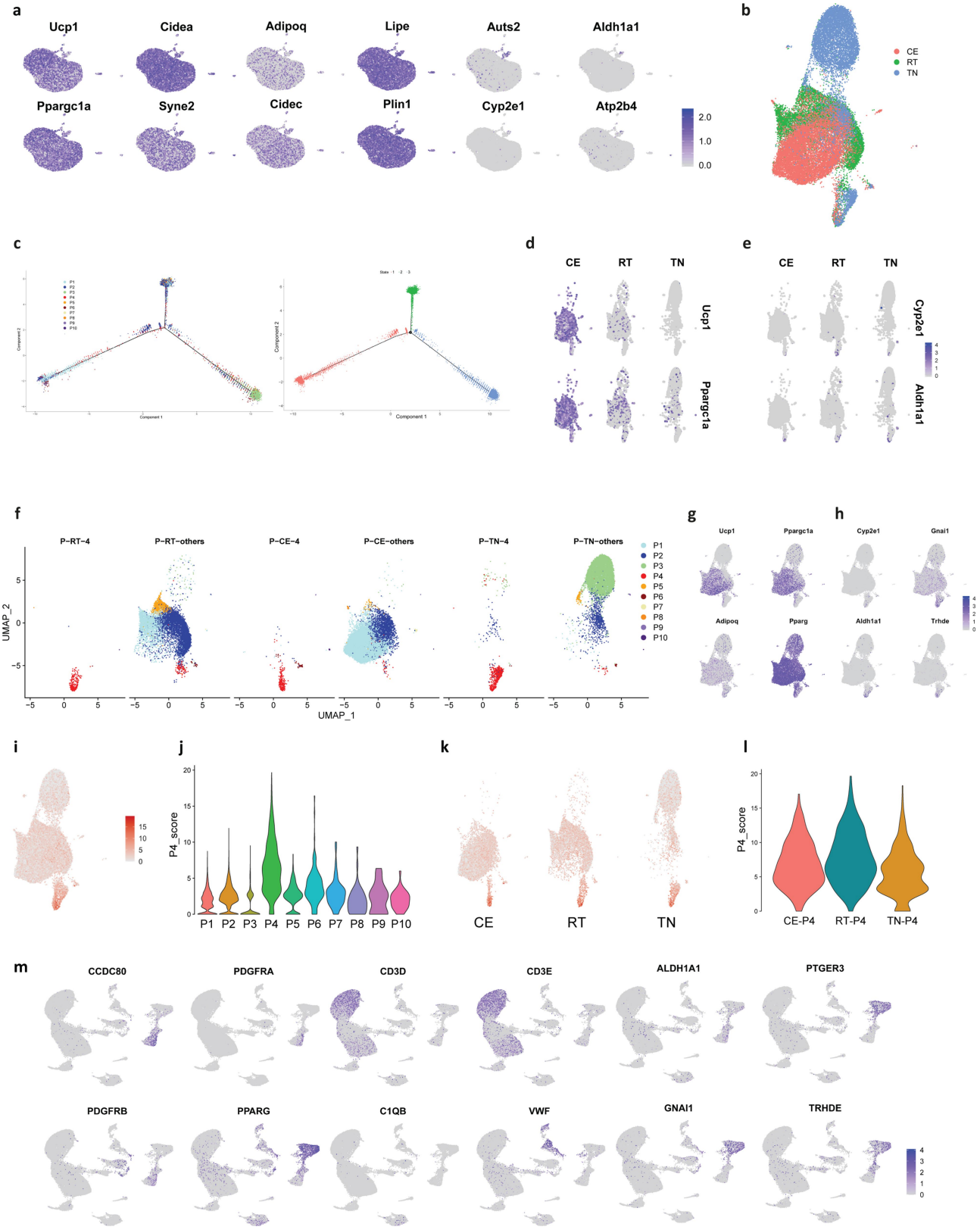

Extended Data Fig. 2 | See next page for caption.

Extended Data Fig. 2 | Dynamics of subpopulations of mouse brown adipocytes under thermoneutral, room-temperature and cold-exposure conditions. a, Mouse iBAT in the cold-exposure condition; feature plots of *Ucp1*, *Cidea*, *Ppargc1a*, *Syne2*, *Adipoq*, *Lipe*, *Cidec*, *Plin1*, *Cyp2e1*, *Auts2*, *Aldh1a1* and *Atp2b4*. **b**–**l**, Integrated analysis of mouse iBAT 10x snRNA-seq data. **b**, UMAP plots of integrated mouse adipocyte nuclei from iBAT grouped by different conditions. **c**, Pseudotime plot of integrated mouse adipocyte nuclei from iBAT by Monocle. **d**, **e**, Feature plots for brown markers *Ucp1*, *Ppargc1a* (**d**) and P4 markers *Cyp2e1*, *Aldh1a1* (**e**), split by different conditions. **f**, P-RT-4, P-CE-4 and P-TN-4 cells shown in the integrated UMAP plot, split by different conditions. **g**, **h**, Feature plots for brown/adipocyte markers *Ucp1*, *Ppargc1a*, *Adipoq* and *Pparg* (**g**) and P4 markers *Cyp2e1*, *Gnai1*, *Aldh1a1* and *Trhde* (**h**). **i**–**l**, P4_score calculates the summation of *Aldh1a1*, *Cyp2e1*, *Auts2*, *Trhde*, *Ptger3*, *Gnai1*, *Asph* and *Cachd1* for each cell. Feature plots for P4_score (**i**), split by conditions (**k**); violin plots for P4_score (**j**), split by different conditions (**l**). **m**, Feature plots for *CCDC80*, *PDGFRA*, *PDGFRB*, *PPARG*, *CD3D*, *CD3E*, *C1QB*, *VWF*, *ALDH1A1*, *PTGER3*, *GNAI1* and *TRHDE* of snRNA-seq for human deep-neck BAT. This figure is related to Fig. 1.

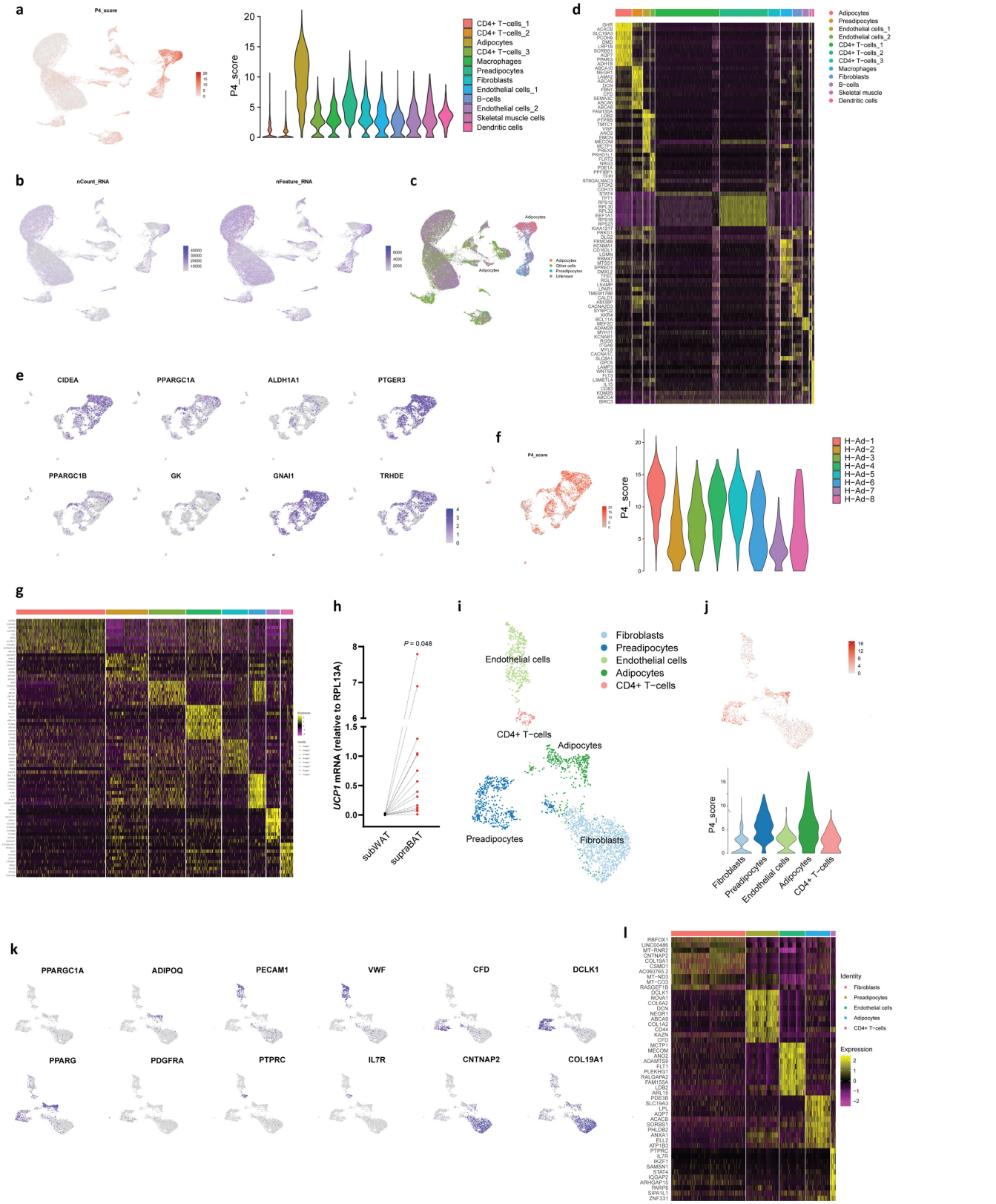

Extended Data Fig. 3 | Identification of subpopulations of human brown and white adipocytes. a–**d**, Feature or violin plots for P4_score (**a**), UMI and gene per nucleus (**b**) or annotation of adipocytes by Garnett classifier[55] (**c**) and heat map (**d**) of snRNA-seq for human deep-neck BAT. P4_score calculates the sum of *ALDH1A1*, *CYP2E1*, *AUTS2*, *TRHDE*, *PTGER3*, *GNAI1*, *ASPH* and *CACHD1* for each cell. **e**–**g**, Feature or violin plots for *CIDEA*, *PPARGC1A*, *PPARGC1B*, *GK*, *ALDH1A1*, *PTGER3*, *GNAI1* and *TRHDE* expression (**e**) or P4_score (**f**) and heat map (**g**) of human brown adipocyte populations. **h**, *UCP1* mRNA level of deep-neck supraclavicular BAT and subcutaneous WAT for each individual. $n = 16$ individuals, $t = 2.2$. **i**, Unsupervised clustering of 2,438 nuclei from human subcutaneous WAT, yielding 608 (median) genes; annotation by SingleR. **j**–**l**, Feature or violin plots for P4_score (**j**) or *PPARGC1A*, *ADIPOQ*, *PPARG*, *PDGFRA*, *PECAM1*, *VWF*, *PTPRC*, *IL7R*, *CFD*, *DCLK1*, *CNTNAP2* and *COL19A1* expression (**k**) and heat map (**l**) of snRNA-seq for human subcutaneous WAT. Statistical significance was calculated using two-tailed paired *t*-test (**h**). This figure is related to Fig. 1.

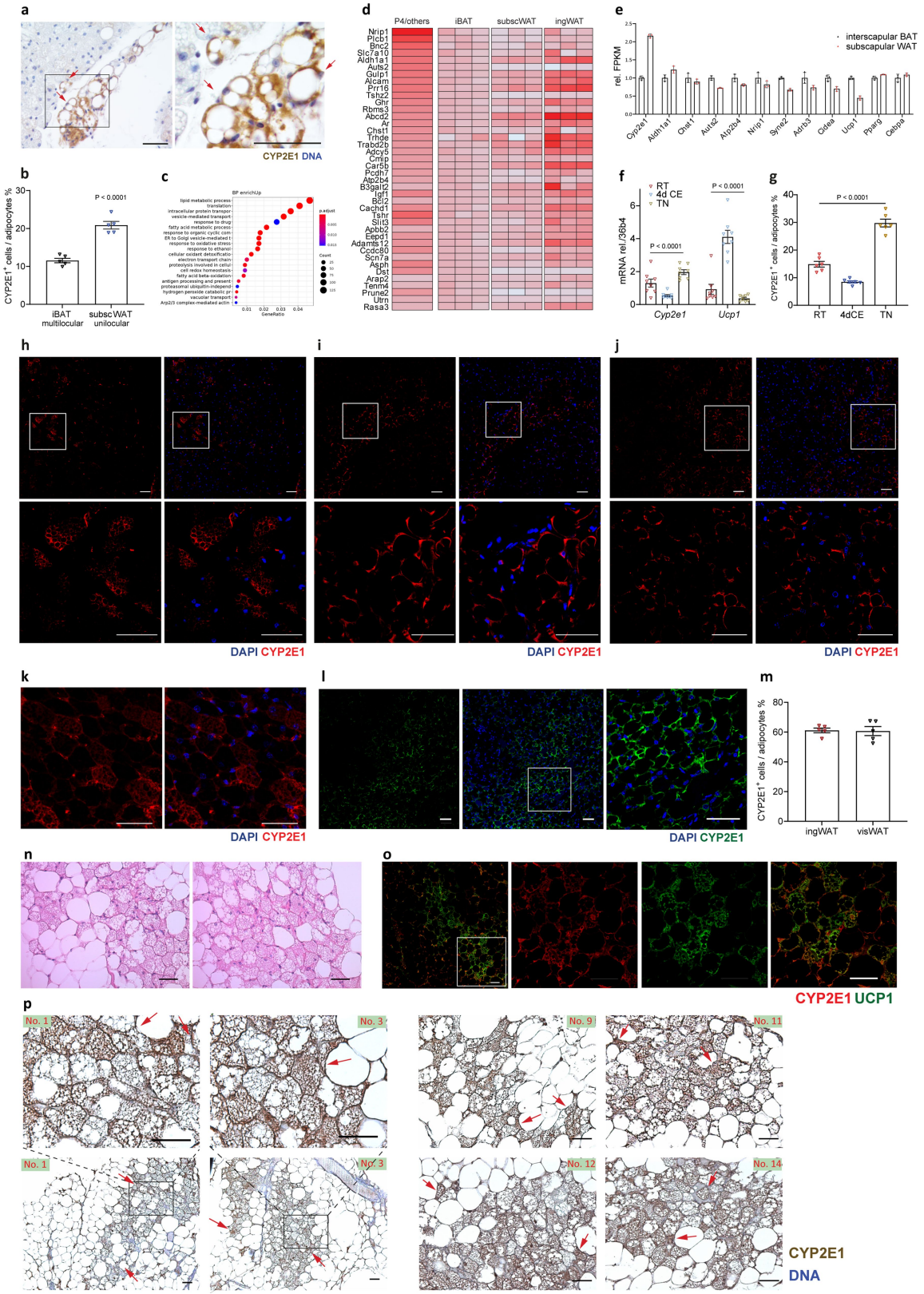

Extended Data Fig. 4 | See next page for caption.

Extended Data Fig. 4 | CYP2E1 marks a specific subpopulation of adipocytes in mouse and human adipose tissue. a, CYP2E1 immunohistochemical staining in iBAT at room temperature. Red arrows indicate CYP2E1-positive staining. **b**, Quantification of $CYP2E1^+$ cells with multilocular and unilocular morphology in the interscapular adipose tissue. $n = 5$ independent experiments, $t = 8.0$. **c**–**e**, Bulk RNA-seq of subscWAT, iBAT and ingWAT. $n = 3$ mice. **c**, Biological pathways enriched in iBAT over subscWAT, analysed by clusterProfiler[56], which calculates a P value using the hypergeometric distribution adjusted for multiple comparison; **d**, Heat map for subscWAT, iBAT and ingWAT of the top-40 P4 markers. **e**, RNA expression level of P4 and adipocyte markers in bulk RNA-seq of iBAT and subscWAT. **f**, mRNA expression levels of *Cyp2e1* and *Ucp1* in mouse iBAT kept in room-temperature, cold-exposure and thermoneutral conditions. $n = 8$ mice, $F_{Cyp2e1} = 18.4$, $F_{Ucp1} = 47.6$. **g**, Quantification of $CYP2E1^+$ cells in mouse iBAT in room-temperature, cold-exposure or thermoneutral conditions. $n = 6$ independent experiments, $F = 112.2$. **h**, CYP2E1 immunofluorescence staining in mouse iBAT after cold exposure. **i**, CYP2E1 immunofluorescence staining in mouse iBAT at thermoneutrality. **j**, CYP2E1 immunofluorescence staining in mouse ingWAT at room temperature. **k**, CYP2E1 immunofluorescence staining in mouse ingWAT after cold exposure. **l**, CYP2E1 immunofluorescence staining in mouse visWAT at room temperature. **m**, Quantification of $CYP2E1^+$ cells in mouse ingWAT and visWAT at room temperature. $n = 5$ independent experiments. **n**, H&E staining of human deep-neck BAT. Two representative images from six individuals. **o**, Immunofluorescence staining of CYP2E1 and UCP1 in human deep-neck BAT. **p**, Immunohistochemical staining of CYP2E1 in human deep-neck BAT for individuals 1, 3, 9, 11, 12 and 14. Red arrows indicate CYP2E1-positive staining. Data are mean average ± s.e.m. Statistical significance was calculated using a two-tailed unpaired Student's t-test (**b**) or one-way ANOVA (**f**, **g**). Scale bars, 50 μm. This figure is related to Fig. 2.

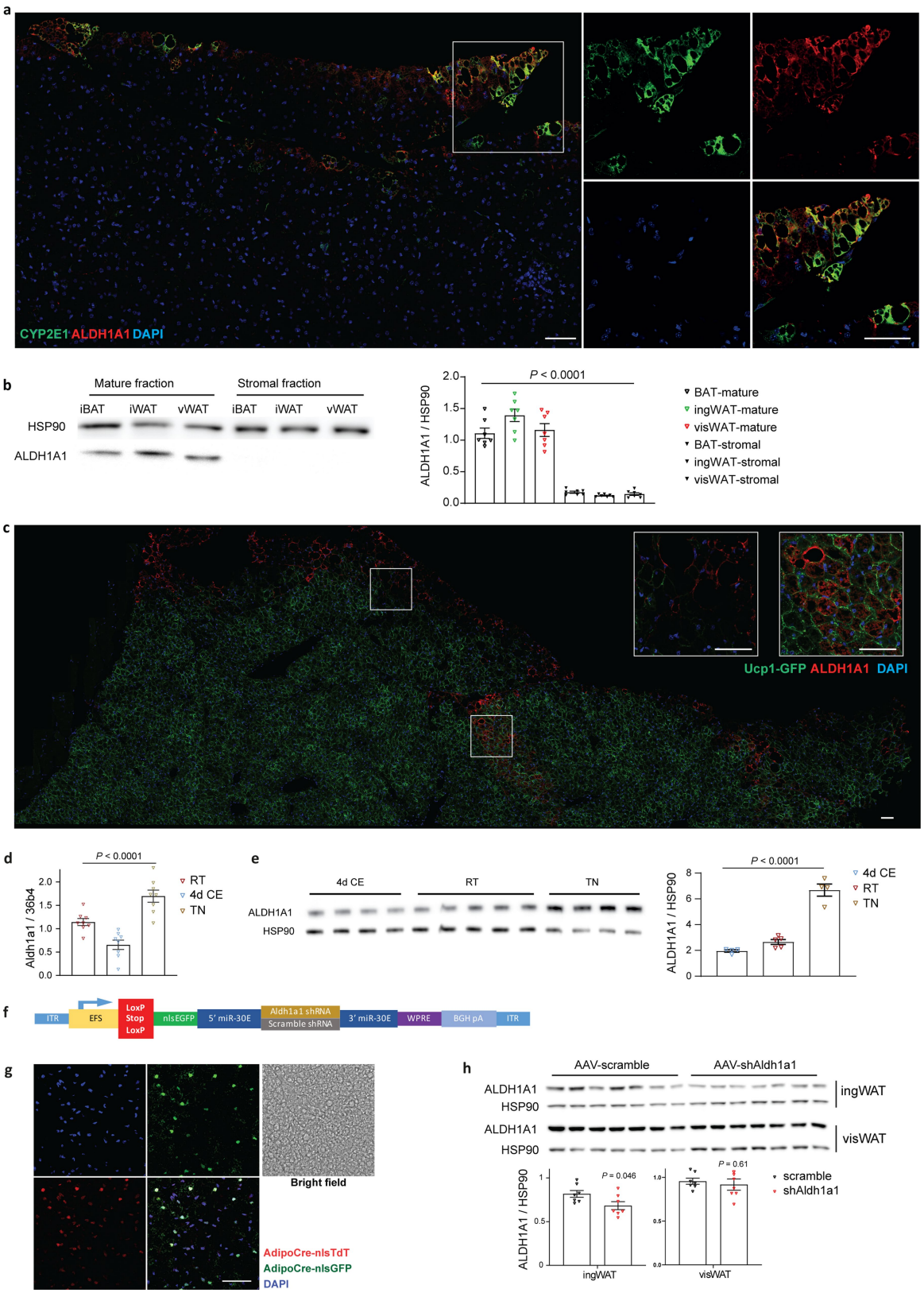

Extended Data Fig. 5 | See next page for caption.

Extended Data Fig. 5 | ALDH1A1 and CYP2E1 are specific markers for the P4 adipocyte subpopulation. a, Immunofluorescence co-staining of CYP2E1 and ALDH1A1 in mouse iBAT at room temperature. **b**, ALDH1A1 protein levels in mature adipocytes and SVF of three adipose tissue depots. $n = 7$ mice, $F = 78.06$, df = 41. **c**, Immunofluorescence staining of ALDH1A1 in the interscapular adipose tissue of Ucp1-GFP transgenic mice at room temperature. **d**, *Aldh1a1* mRNA expression levels of mouse iBAT in room-temperature, cold-exposure or thermoneutral conditions. $n = 8$ mice, $F = 25.1$. **e**, ALDH1A1 protein expression levels of mouse iBAT in room-temperature, cold-exposure or thermoneutral conditions. $n = 4$ mice (except $n = 5$ for the room-temperature cohort), $F = 75.6$. **f**, Schematic map of the AAV knockdown constructs. **g**, Confocal images of mouse iBAT from AAV-injected mice. **h**, Immunoblot of ALDH1A1 in ingWAT ($n = 7$ mice, $t = 2.23$) and visWAT ($n = 7$ mice, $t = 0.53$) after injection of shRNA AAV into iBAT. Data are mean average ± s.e.m. Statistical significance was calculated using a one-way ANOVA (**b**, **d**, **e**) or two-tailed unpaired Student's *t*-test (**h**). Scale bars, 50 μm. See gel source data in Supplementary Fig. 1a, d, e. This figure is related to Fig. 3.

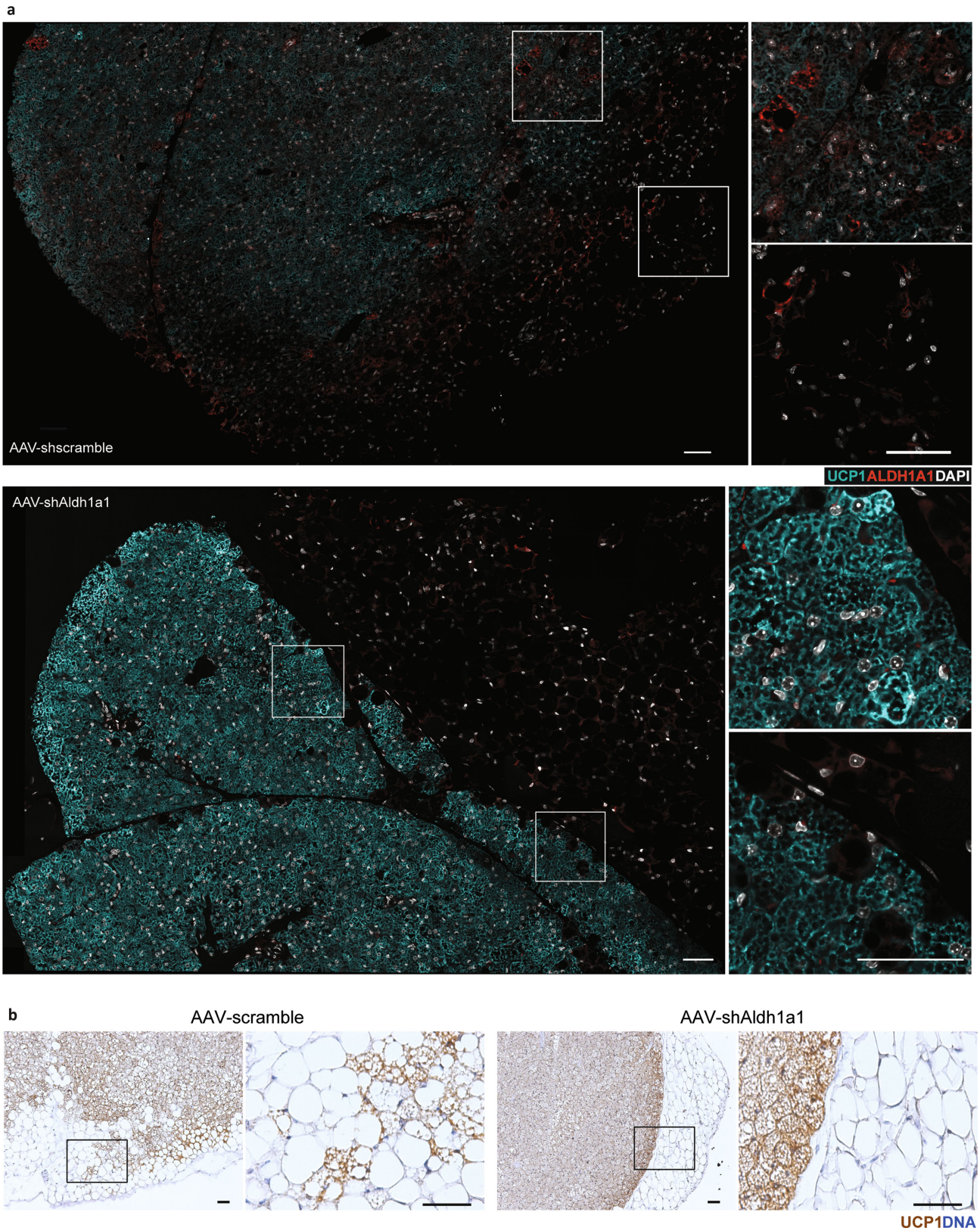

Extended Data Fig. 6 | Reduction of ALDH1A1 expression in BAT regulates UCP1 expression in BAT. a, Immunofluorescence staining of ALDH1A1 in iBAT of AAV-injected mice after cold exposure. Representative image from four independent experiments. **b**, Immunohistochemical staining of UCP1 in subscWAT from shRNA-AAV-injected mice after cold exposure. Representative image from four independent experiments. Scale bars, 50 μm. This figure is related to Fig. 3.

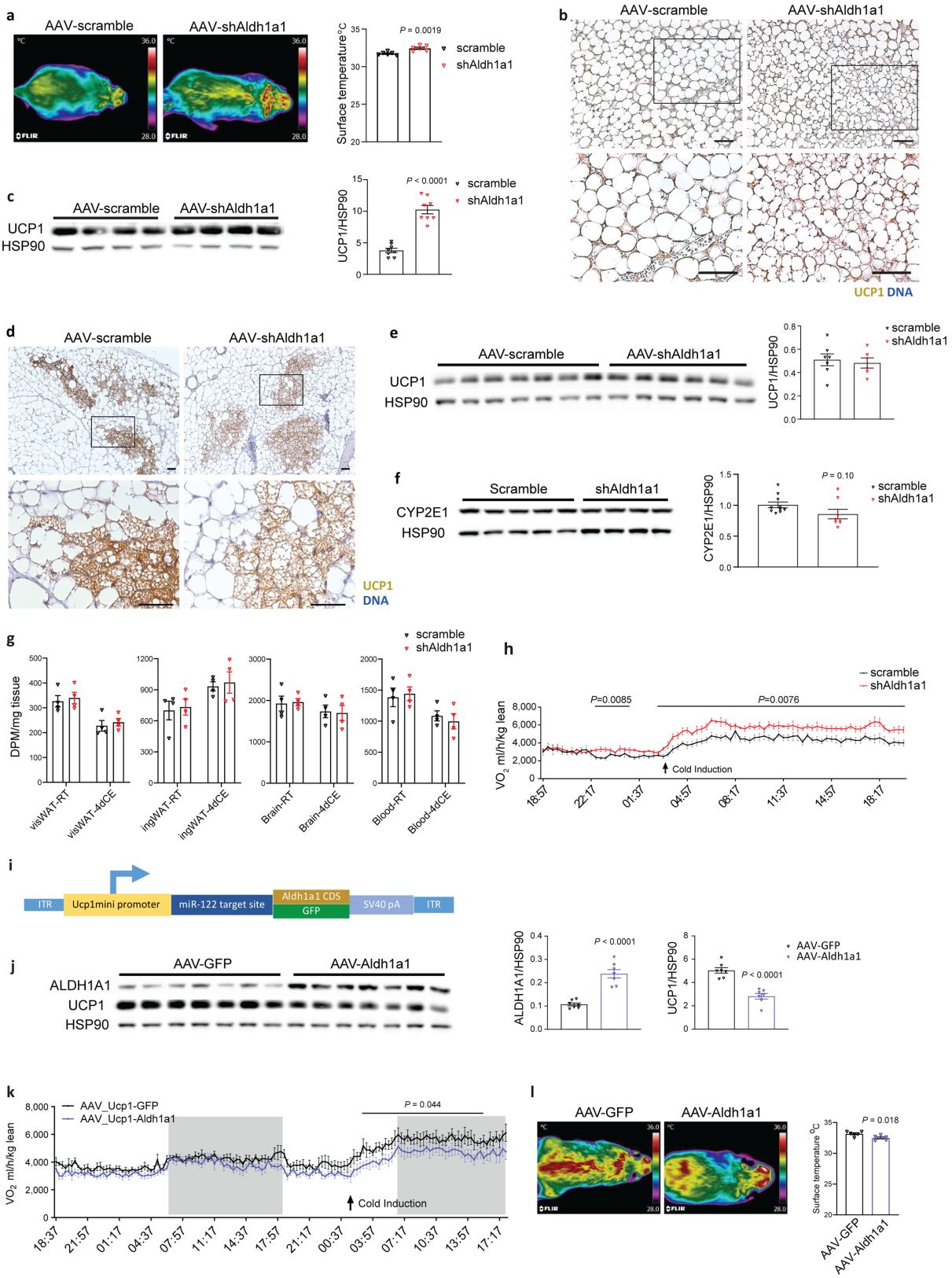

Extended Data Fig. 7 | See next page for caption.

Extended Data Fig. 7 | Reduction of ALDH1A1 expression in BAT induces BAT thermogenic capacity. a, Surface temperature of iBAT shRNA-AAV-injected mice at thermoneutrality. $n = 6$ mice, $t = 4.17$, df = 10. **b**, Immunohistochemical staining of UCP1 in iBAT of iBAT shRNA-AAV-injected mice at thermoneutrality. **c**, Protein levels of UCP1 in iBAT of iBAT shRNA-AAV-injected mice at thermoneutrality. $n = 8$ mice, $t = 8.58$, df = 14. **d**, Immunohistochemical staining of UCP1 in ingWAT of shRNA-AAV-injected mice after cold exposure. **e**, UCP1 protein levels in ingWAT from shRNA-AAV-injected mice after cold exposure. $n_{shAldh1a1} = 6$ mice, $n_{scramble} = 7$ mice. **f**, CYP2E1 protein levels in iBAT from shRNA-AAV-injected mice at room temperature. $n_{shAldh1a1} = 8$ mice, $n_{scramble} = 10$ mice. **g**, Glucose uptake of ingWAT, visWAT, brain and blood in mice injected with iBAT shRNA AAV. $n = 4$ mice. **h**, Time-resolved oxygen consumption of AAV-injected mice after cold exposure. $n = 5$ mice, df = 8, $t_{RT} = 2.57$, $t_{CE} = 2.33$. **i**, Schematic illustration of the overexpression AAV construct with mini *Ucp1* promoter. **j**, ALDH1A1 and UCP1 protein levels of iBAT from iBAT AAV-*GFP*- or AAV-*Aldh1a1*-injected mice. $n = 7$ mice, df = 12, $t_{ALDH1A1} = 6.8$ $t_{UCP1} = 6.6$. **k**, Time-resolved oxygen consumption of iBAT AAV-*GFP*- or AAV-*Aldh1a1*-injected mice after cold exposure. $n = 5$ mice. **l**, Surface temperature of iBAT AAV-*GFP*- or AAV-*Aldh1a1*-injected mice at room temperature. $n = 6$ mice, $t = 2.8$, df = 10. Data are mean average ± s.e.m. Statistical significance was calculated using a two-tailed unpaired Student's *t*-test. Scale bars, 50 µm. See gel source data in Supplementary Figs. 1f, g, 2a, b. This figure is related to Fig. 3.

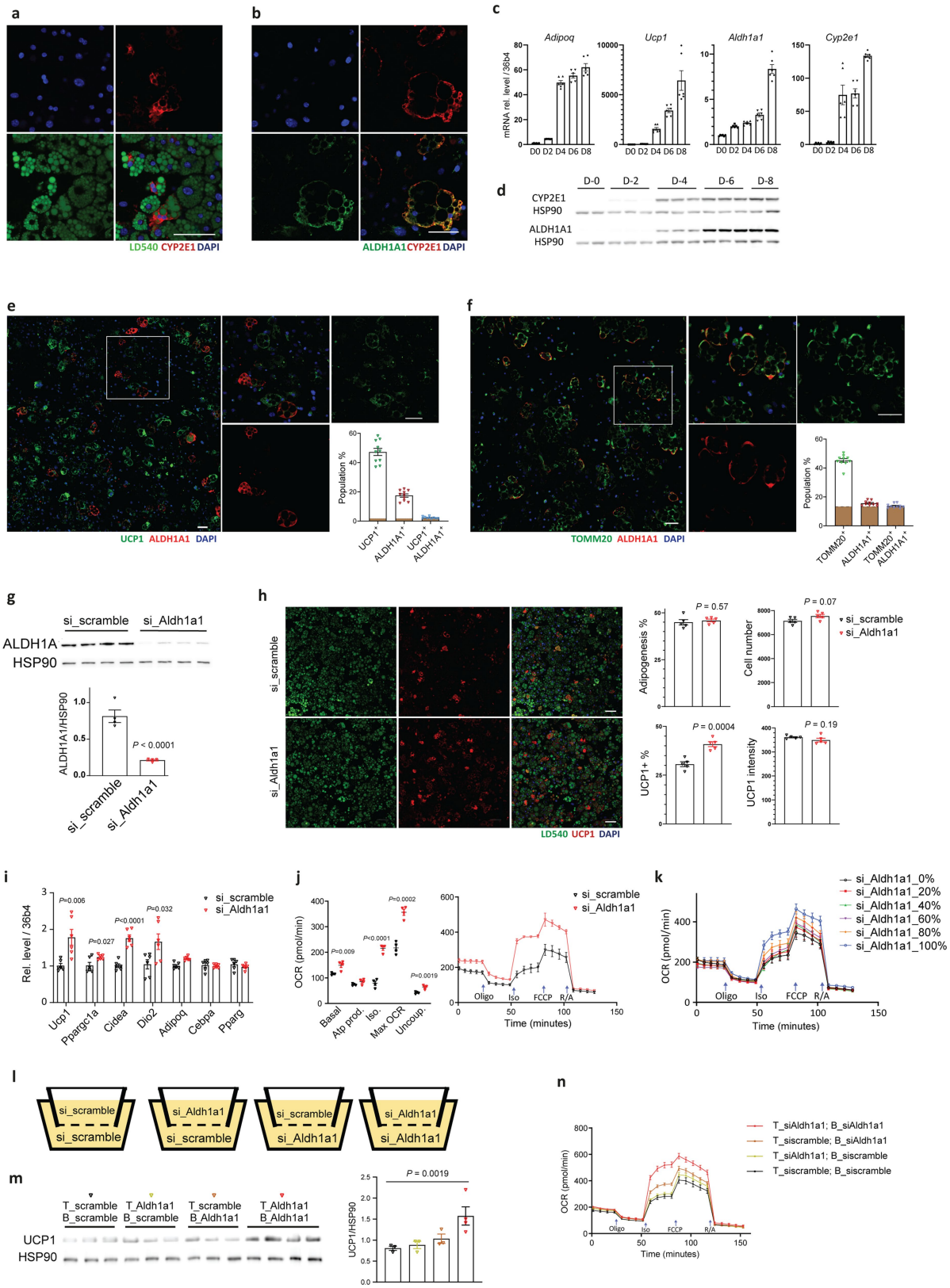

Extended Data Fig. 8 | See next page for caption.

Extended Data Fig. 8 | Reduction of ALDH1A1 during brown adipocyte formation induces thermogenic capacity. a, Immunofluorescence staining and quantification of CYP2E1 and LD540 in ex-vivo-differentiated cells from iBAT. **b**, Immunofluorescence staining of ALDH1A1 and CYP2E1 in ex-vivo-differentiated cells from ingWAT. **c**, mRNA level of *Adipoq*, *Ucp1*, *Cyp2e1* and *Aldh1a1* during brown adipocyte differentiation ex vivo. $n = 6$ independent experiments. **d**, Protein levels of CYP2E1 and ALDH1A1 during brown adipocyte differentiation ex vivo. **e**, Immunofluorescence staining and quantification of ALDH1A1 and UCP1 in ex-vivo-differentiated adipocytes from iBAT. Brown area in the quantification bar plot denotes the overlap of $UCP1^+ALDH1A1^+$ double-positive population. $n = 10$ independent experiments. **f**, Immunofluorescence staining of ALDH1A1 and TOMM20 in ex-vivo-differentiated cells from iBAT. Brown area in the quantification bar plot denotes the overlap of $TOMM20^+ALDH1A1^+$ double-positive population. $n = 10$ independent experiments. **g**, Protein levels of ALDH1A1 in ex-vivo-differentiated cells from iBAT after *Aldh1a1*-siRNA-mediated knockdown. $n = 4$ independent experiments, $t = 6.97$, df = 6. **h**, Immunofluorescence staining of UCP1 and LD540 in ex-vivo-differentiated cells from iBAT after *Aldh1a1*-siRNA-mediated knockdown. $n = 5$ independent experiments, $t_{UCP1+\%} = 5.73$, df = 8. **i**, mRNA levels of *Ucp1*, *Ppargc1a*, *Cidea*, *Dio2*, *Adipoq*, *Cebpa* and *Pparg* in ex-vivo-differentiated cells from iBAT after *Aldh1a1*- and scramble-siRNA knockdown. $n = 6$ independent experiments, df = 10, $t_{Ucp1} = 3.46$, $t_{Ppargc1a} = 2.59$, $t_{Cidea} = 7.30$, $t_{Dio2} = 2.49$. **j**, Cellular respiration (OCR) after siRNA-mediated knockdown in brown adipocytes. $n = 4$ independent experiments, df = 6, $t_{Basal} = 3.82$, $t_{Atp} = 2.14$, $t_{Iso} = 12.2$, $t_{Max} = 8.39$, $t_{Uncoupling} = 5.28$. **k**, Time-resolved OCR of ex-vivo-differentiated cells from iBAT. Cells transfected with *Aldh1a1* or scramble siRNA were mixed in different ratios (related to Fig. 4d). **l**, Schematic illustration of the co-culture experiment. Cells transfected with *Aldh1a1* or scrambled siRNA were cultured in the bottom or top chamber as indicated. **m**, UCP1 protein level of co-cultured cells in the bottom well. $n = 4$ independent experiments, $F = 5.64$. **n**, Cellular respiration of co-cultured cells in the bottom well. $n = 5$ independent experiments. Data are mean average ± s.e.m. Statistical significance was calculated using a two-tailed unpaired Student's *t*-test (**g**–**i**) or ordinary one-way ANOVA (**m**). Scale bars, 50 µm. See gel source data in Supplementary Fig. 2c, d. This figure is related to Fig. 4.

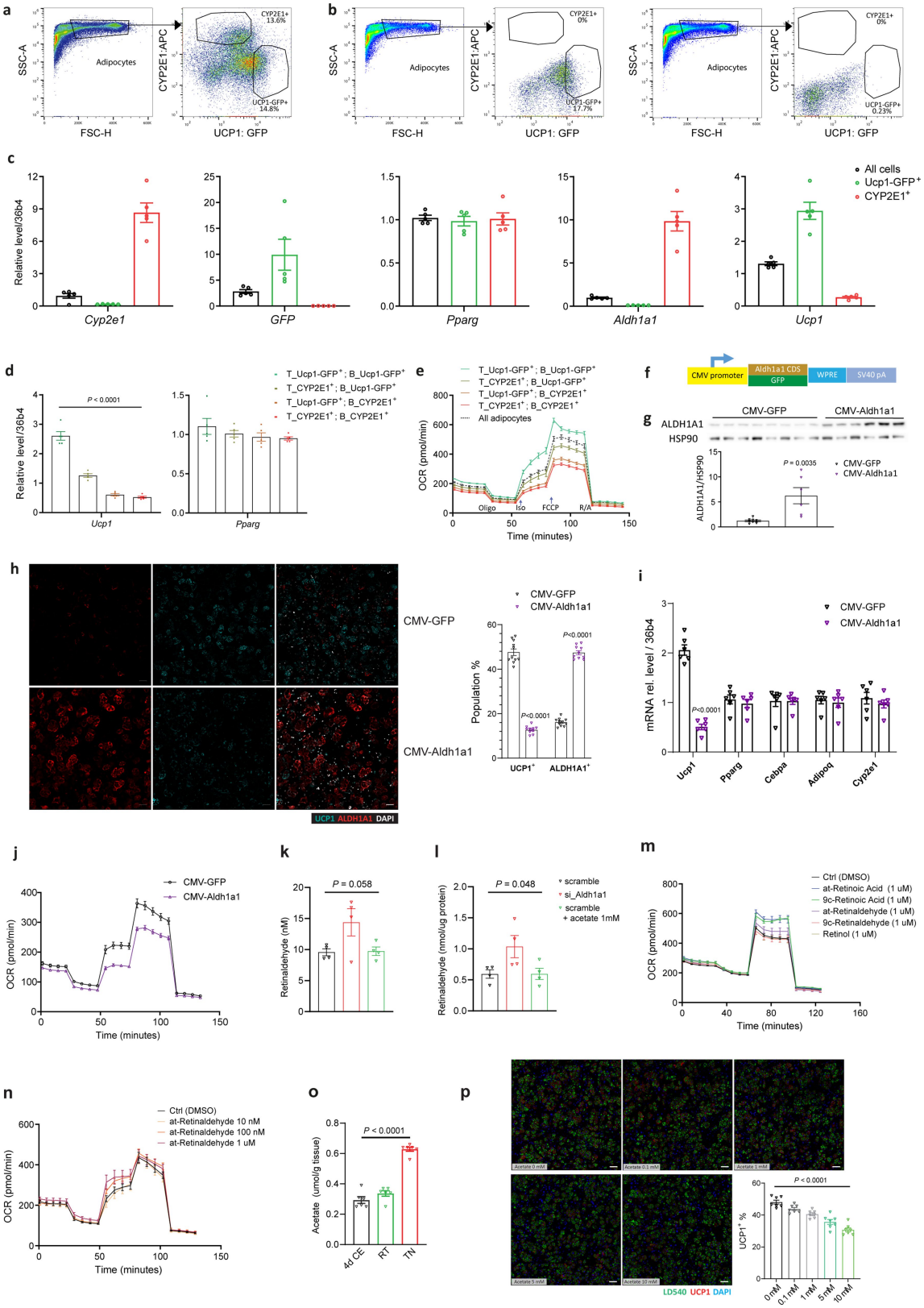

Extended Data Fig. 9 | See next page for caption.

Extended Data Fig. 9 | Overexpression of ALDH1A1 during brown adipocyte formation reduces thermogenic capacity. a, **b**, FACS gating of adipocytes, $CYP2E1^+$ and GFP^+ cells from ex-vivo-differentiated adipocytes (**a**), and FACS control for the CYP2E1 antibody (left) and GFP (right) (**b**). **c**, mRNA expression levels of *Cyp2e1*, *GFP*, *Pparg*, *Aldh1a1* and *Ucp1* in FACS-sorted cells. $n = 5$ independent experiments. **d**, mRNA expression levels of *Ucp1* and *Pparg* in FACS and co-cultured cells. $n = 5$ independent experiments, $F_{Ucp1} = 134.7$, $F_{Pparg} = 1.2$. **e**, Time-resolved cellular respiration of FACS selected and co-cultured cells (related to Fig. 4e). **f**, Schematic illustration of the overexpression lentiviral construct with mini *CMV* promoter, based on pLenti-MP2[57]. **g**, Protein levels of ALDH1A1 in ex-vivo-differentiated cells from iBAT infected with AAV-*GFP* or AAV-*Aldh1a1*. $n_{GFP} = 8$ independent experiments, $n_{Aldh1a1} = 6$ independent experiments, $t = 3.62$. **h**, Immunofluorescence staining of ALDH1A1 and UCP1 in ex vivo differentiated cells from iBAT infected with AAV-*GFP* or AAV-*Aldh1a1*, $n_{GFP} = 11$ independent experiments, $n_{Aldh1a1} = 10$ independent experiments, $t_{UCP1+} = 21.4$, $t_{ALDH1A1+} = 30.1$. (**i**) mRNA expression levels of *Ucp1*, *Pparg*, *Cebpa*, *Adipoq* and *Cyp2e1* in ex-vivo-differentiated cells from iBAT infected with AAV-*GFP* or AAV-*Aldh1a1*. $n = 6$ independent experiments, $t_{Ucp1} = 13.1$. **j**, Cellular respiration of *Aldh1a1*- or *GFP*-overexpressing cells. $n = 6$ independent experiments. **k**, Retinaldehyde quantification in the supernatant of ex-vivo-differentiated cells from iBAT, treated with the indicated siRNA and/or acetate. $n = 4$ independent experiments, $F = 3.99$, $P = 0.058$. **l**, Retinaldehyde quantification of intracellular abundance of retinaldehyde in ex-vivo-differentiated cells from iBAT, treated with the indicated siRNA and/or acetate. $n = 4$ independent experiments, $F = 4.348$, $P = 0.048$. **m**, Cellular respiration of ex-vivo-differentiated cells from iBAT, treated with the indicated retinoids. $n = 5$ independent experiments. **n**, Cellular respiration of ex-vivo-differentiated cells from iBAT, treated with all-trans retinaldehyde at the indicated concentrations. $n = 5$ independent experiments. **o**, Acetate levels in iBAT of mice kept in cold-exposure, room-temperature and thermoneutral conditions. $n = 6$ independent experiments, $F = 97.79$. **p**, UCP1 and LD540 staining in ex-vivo-differentiated cells from iBAT, treated with the indicated levels of acetate during differentiation from day 4 to 8. $n = 7$ independent experiments, $t = 32.4$. Data are mean average ± s.e.m. Statistical significance was calculated using a one-way ANOVA (**d**, **k**, **l**, **o**, **p**) or two-tailed unpaired Student's *t*-test (**g**–**i**). Scale bars, 50 µm. See gel source data in Supplementary Fig. 2f. This figure is related to Fig. 4.

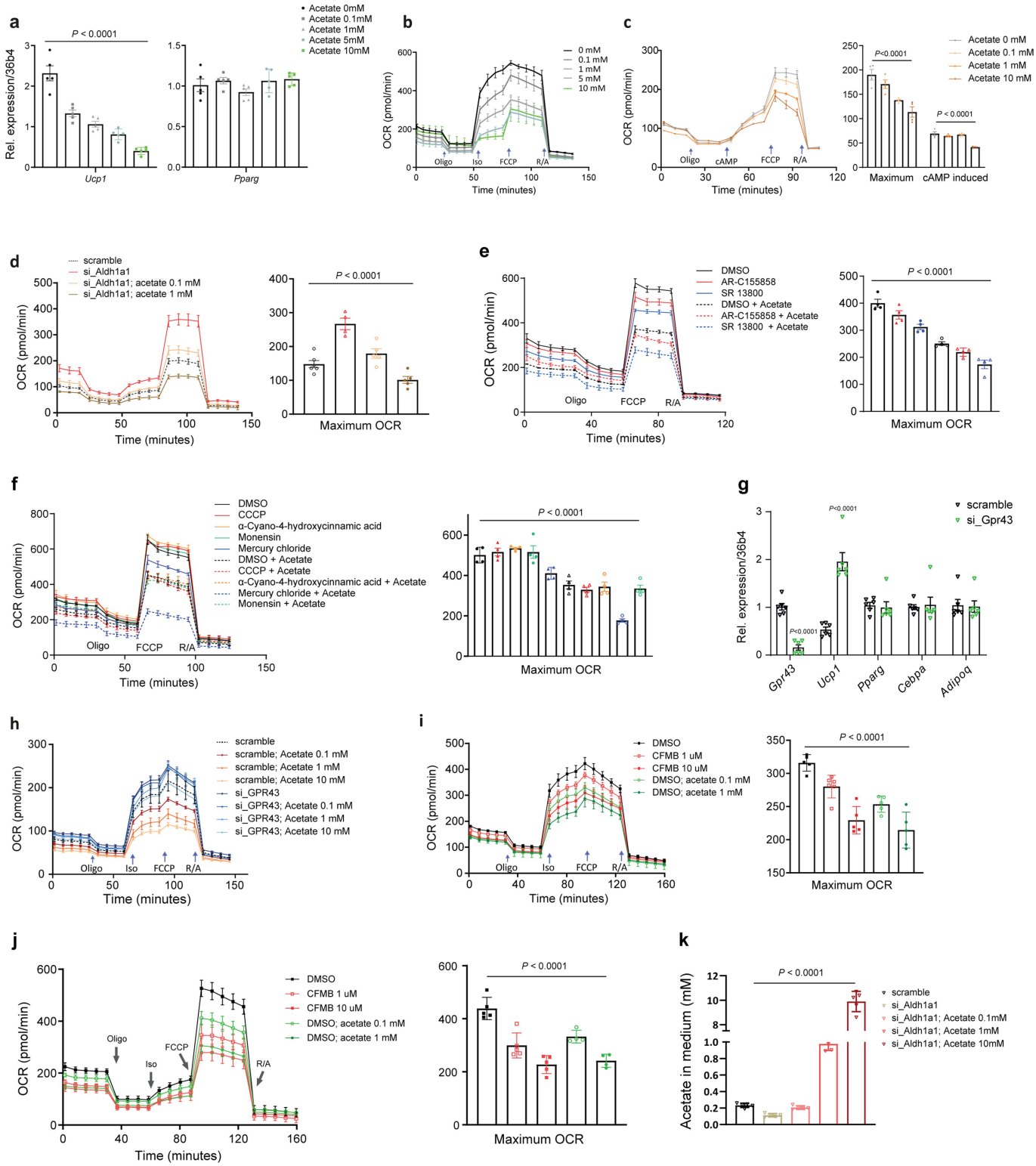

Extended Data Fig. 10 | See next page for caption.

Extended Data Fig. 10 | ALDH1 regulates brown adipocyte thermogenic capacity through acetate signalling. a, *Ucp1* and *Pparg* mRNA expression levels in ex-vivo-differentiated cells from iBAT, treated with various levels of acetate during differentiation from day 4 to 8. $n = 5$ independent experiments, $t = 50.7$. **b**, Time-resolved cellular respiration in ex-vivo-differentiated cells from iBAT treated with the indicated levels of acetate (related to Fig. 4g). **c**, Cellular respiration in differentiated human MADS treated with the indicated levels of acetate during differentiation from day 16 to 17. $n = 4$ independent experiments (except $n = 5$ for the acetate 1 mM cohort), $F_{Max} = 16.2$, $F_{cAMP} = 32.95$. **d**, Cellular respiration in ex-vivo-differentiated cells from iBAT treated with the indicated levels of acetate in the presence or absence of *Aldh1a1* knockdown. $n = 5$ independent experiments, $F = 22.7$. **e**, Cellular respiration in ex-vivo-differentiated cells from iBAT, treated with acetate (1 mM), AR-C155858 (1 µM) or SR13800 (1 µM). $n = 4$ independent experiments, $F_{Max} = 49.6$. **f**, Cellular respiration in ex-vivo-differentiated cells from iBAT, treated with acetate (1 mM), CCCP (1 µM), α-cyano-4-hydroxycinnamic acid (1 mM), monensin (10 µM) or mercury chloride (5 µM). $n = 4$ independent experiments, $F_{Max} = 39.1$. **g**, *Gpr43*, *Ucp1*, *Pparg*, *Cebpa* and *Adipoq* mRNA expression levels in ex-vivo-differentiated cells from iBAT with *Gpr43* knockdown. $n = 6$ independent experiments, $t_{Gpr43} = 9.5$, $t_{Ucp1} = 7.2$. **h**, Time-resolved cellular respiration in brown adipocytes treated with the indicated levels of acetate with or without *Gpr43* knockdown (related to Fig. 4h). **i**, Cellular respiration in ex-vivo-differentiated cells from iBAT, treated with the indicated levels of acetate and the GPR43 agonist CFMB. $n = 5$ independent experiments (except $n = 6$ for the CFMB 1 µM cohort), $F = 23.9$. **j**, Cellular respiration in ex-vivo-differentiated cells from ingWAT, treated with the indicated levels of acetate and GPR43 agonist. $n = 5$ independent experiments (except $n = 4$ for DMSO; acetate 0.1 mM and DMSO; acetate 1 mM cohorts), $F_{Max} = 25.8$. **k**, Acetate levels in the culture medium of in ex-vivo-differentiated cells from iBAT with *Aldh1a1* knockdown, treated with the indicated levels of acetate. $n = 5$ independent experiments, $F = 652.7$. Data are mean average ± s.e.m. Statistical significance was calculated using a one-way ANOVA (**a**, **c**–**f**, **i**–**k**) or two-tailed unpaired Student's *t*-test (**g**). This figure is related to Fig. 4.

nature research

Corresponding author(s): Christian Wolfrum, Wenfei Sun

Last updated by author(s): July 11, 2020

Reporting Summary

Nature Research wishes to improve the reproducibility of the work that we publish. This form provides structure for consistency and transparency in reporting. For further information on Nature Research policies, see our Editorial Policies and the Editorial Policy Checklist.

Statistics

For all statistical analyses, confirm that the following items are present in the figure legend, table legend, main text, or Methods section.

n/a	Confirmed	
☐	☒	The exact sample size (*n*) for each experimental group/condition, given as a discrete number and unit of measurement
☐	☒	A statement on whether measurements were taken from distinct samples or whether the same sample was measured repeatedly
☐	☒	The statistical test(s) used AND whether they are one- or two-sided *Only common tests should be described solely by name; describe more complex techniques in the Methods section.*
☐	☒	A description of all covariates tested
☐	☒	A description of any assumptions or corrections, such as tests of normality and adjustment for multiple comparisons
☐	☒	A full description of the statistical parameters including central tendency (e.g. means) or other basic estimates (e.g. regression coefficient) AND variation (e.g. standard deviation) or associated estimates of uncertainty (e.g. confidence intervals)
☐	☒	For null hypothesis testing, the test statistic (e.g. *F*, *t*, *r*) with confidence intervals, effect sizes, degrees of freedom and *P* value noted *Give P values as exact values whenever suitable.*
☒	☐	For Bayesian analysis, information on the choice of priors and Markov chain Monte Carlo settings
☐	☒	For hierarchical and complex designs, identification of the appropriate level for tests and full reporting of outcomes
☐	☒	Estimates of effect sizes (e.g. Cohen's *d*, Pearson's *r*), indicating how they were calculated

Our web collection on statistics for biologists contains articles on many of the points above.

Software and code

Policy information about availability of computer code

Data collection	We used Illumina Nextseq 500 (smartseq2 libraries) and Novaseq 6000 (10x libraries) to acquired RNAseq data.
Data analysis	We applied CellRanger V3.0 to generate gene expression matrix, CellBender to adjust for ambient RNA, Scrublet and DoubletFinder to remove potential doublets, Seurat (V3.1.1) to correct batch effect and cell clustering, Monocle (V2) and velocyto for cell trajectory modeling, SingleR to annotate cell, Flow Jo (10.4.2) for FACS data analysis, ImageJ (Fiji 1.51) for western blots quantification, Harmony 3.5 for Operetta image analysis.

For manuscripts utilizing custom algorithms or software that are central to the research but not yet described in published literature, software must be made available to editors and reviewers. We strongly encourage code deposition in a community repository (e.g. GitHub). See the Nature Research guidelines for submitting code & software for further information.

Data

Policy information about availability of data

All manuscripts must include a data availability statement. This statement should provide the following information, where applicable:

- Accession codes, unique identifiers, or web links for publicly available datasets
- A list of figures that have associated raw data
- A description of any restrictions on data availability

All RNA sequencing data is deposited in ArrayExpress: E-MTAB-8561 for single-nucleus RNAseq of mouse brown adipocytes at RT by SMARTseq2; E-MTAB-8562 for single-nucleus RNAseq of mouse brown adipocytes at RT, CE, TN by 10x; E-MTAB-8564 for single-nucleus RNAseq of human BAT cells by 10x; E-MTAB-9192 for subscapular WAT, iBAT, ingWAT bulk RNAseq; E-MTAB-9199 for snRNAseq of human subcutaneous WAT cells;

Field-specific reporting

Please select the one below that is the best fit for your research. If you are not sure, read the appropriate sections before making your selection.

☒ Life sciences ☐ Behavioural & social sciences ☐ Ecological, evolutionary & environmental sciences

For a reference copy of the document with all sections, see nature.com/documents/nr-reporting-summary-flat.pdf

Life sciences study design

All studies must disclose on these points even when the disclosure is negative.

Sample size	Sample sizes were determined on the basis of previous experiments using similar methods (ref. 16,22). Samples size of the human cohort was dependent on the availability of subjects, individual number and cell coverage are larger as previous reports (ref. 23).
Data exclusions	No samples were excluded from any analyses.
Replication	Experimental findings were verified by biological replicates and technical replicates, each experiment was performed multiple times as indicated in the figure legends.
Randomization	All experiments were randomly allocated to groups.
Blinding	The investigators were not blinded to the mice as they themselves were treating and sacrificing the mice. However, the investigators were blind with sample processing and data analysis.

Reporting for specific materials, systems and methods

We require information from authors about some types of materials, experimental systems and methods used in many studies. Here, indicate whether each material, system or method listed is relevant to your study. If you are not sure if a list item applies to your research, read the appropriate section before selecting a response.

Materials & experimental systems

n/a	Involved in the study
☐	☒ Antibodies
☐	☒ Eukaryotic cell lines
☒	☐ Palaeontology and archaeology
☐	☒ Animals and other organisms
☐	☒ Human research participants
☒	☐ Clinical data
☒	☐ Dual use research of concern

Methods

n/a	Involved in the study
☒	☐ ChIP-seq
☐	☒ Flow cytometry
☒	☐ MRI-based neuroimaging

Antibodies

Antibodies used	Anti UCP1 (#ab10983, Abcam, 1:2000 for WB, 1:500 for IHC/IF), Anti CYP2E1(#ab28146, Abcam, 1:1000 for WB, 1:200 for IHC/IF), Anti ALDH1A1(#ab9883, Abcam, 1:200 for IF), Anti HSP90 (# 4877, CST, 1:1000 for WB), Anti ALDH1A1(#52492, Abcam, 1:1000 for WB, 1:200 for IF), Alexa 488 anti rabbit (# A-21206, ThermoFisher, 1:500 for IF), Alexa 488 anti rabbit (# A-21206, ThermoFisher, 1:500 for IF), Alexa 647 anti rabbit (A-31573, ThermoFisher, 1:500 for IF), Alexa 568 anti goat (# A-11057, ThermoFisher, 1:500 IF), Goat Anti-Rabbit IgG Antibody, HRP-conjugate (12-348, Merck, 1:5000 for WB)
Validation	Anti-UCP1 antibody was validated by a previous study (doi.org/10.1038/s42255-019-0101-4); Anti CYP2E1(#ab28146) was validated by a prevous study (10.1016/j.cell.2018.11.012); Anti-ALDH1A1 antibody (ab9883) was validated by a previous study (doi: 10.7554/eLife.32358.) Anti ALDH1A1(#52492) was validated by a previous study (10.1038/s41467-019-11235-4)

Eukaryotic cell lines

Policy information about cell lines

Cell line source(s)	293-AAV and 293-LTV cell lines were purchased from Cell Biolabs Inc. (cat. AAV-100; LTV-100); hMADS cells were prevously established by our lab (ref. 42).
Authentication	293-AAV and 293-LTV cells were not authenticated, however the AAV and LV produced from these cells were authenticated by PCR. hMADS cells were previously validate by gene expression and functional assay (OCR).
Mycoplasma contamination	The cells are regularly tested, all cell lines tested are negative for mycoplasma contamination.

Commonly misidentified lines (See ICLAC register)	No commonly misidentified cell lines were used in the study.

Animals and other organisms

Policy information about studies involving animals; ARRIVE guidelines recommended for reporting animal research

Laboratory animals	B6;FVB-Tg(Adipoq-cre)1Evdr/J were used, 129-Gt(ROSA)26Sortm7(CAG-tdTomato*)Nat/J were used, C57Bl/6 male mice were used. Male mice at 7-9 weeks of age were used for experiment, except 22 weeks mice for TN experiments. Animals were housed in 23 oC (except 8 oC for CE and 30 oC for TN), with free access to water and food, at a reversed light cycle (7 - 19 dark), at 40% humidity.
Wild animals	No wild animals were used in the study.
Field-collected samples	No field collected samples were used in the study.
Ethics oversight	All experiments were approved by the Animal Ethics Committee of Zurich, all animal studies were approved by the Veterinäramt Zürich.

Note that full information on the approval of the study protocol must also be provided in the manuscript.

Human research participants

Policy information about studies involving human research participants

Population characteristics	Deep neck BAT samples were collected from 16 individuals (4 male/12 female; 49.2 ± 19.0 years (22 – 77 years); BMI 24.8 ± 4.7 kg/m2 (16.9 – 35.2 kg/m2) ; body fat 29.1 ± 8.5 % (15.6 – 46.6 %); thyroid surgery n=14 or branchial cleft cyst surgery n=2; data are expressed as mean ± SD). Patients with malignant disease and subjects younger than 18 years were excluded from participation in the study.
Recruitment	All study participants provided witnessed written informed consent prior entering the study, individuals without malignant disease and subjects older than 18 years are all included, no other selection was applied.
Ethics oversight	The study was approved by the Local Ethics Committee (University Hospital in Bratislava, Slovakia) and it conforms to the ethical guidelines of the 2000 Helsinki declaration.

Note that full information on the approval of the study protocol must also be provided in the manuscript.

Flow Cytometry

Plots

Confirm that:

☒ The axis labels state the marker and fluorochrome used (e.g. CD4-FITC).

☒ The axis scales are clearly visible. Include numbers along axes only for bottom left plot of group (a 'group' is an analysis of identical markers).

☒ All plots are contour plots with outliers or pseudocolor plots.

☒ A numerical value for number of cells or percentage (with statistics) is provided.

Methodology

Sample preparation	Details are available in methods - Nuclei isolation from mouse tissue. Briefly, Interscapular brown adipose tissue was harvested from seven-week-old AdipoCre-NucRed transgenic mice for each experiment. Tissue was minced to 1 mm3 and homogenized in Nuclei EZ Lysis Buffer on ice and filtered through a 40 um cell strainer. This was followed by centrifugation at 500 g for 5 minutes at 4 °C and the pellet was resuspended in PBS. Resuspended nuclei were loaded to MoFlo Astrios EQ Cell Sorter and RFP+ nuclei were collected. On differentiation day 7, Ucp1-GFP iBAT derived cells were detached from a P10 dish by incubation with collagenase (1 mg/ml) in collagenase buffer for 30 min at 37 °C. The cell resuspension was centrifuged for 5 min at 300 g, and the cell pellets was resupended in 20 ml FACS buffer. Cell suspension was filtered through 100 µm cell strainers and centrifuged at 300 g for another 5 min. After removal of the supernatant and resuspension of the cell pellet in FACS buffer to 0.5 X 107 cells/ml cells were incubated with anti-mouse CYP2E1-APC (1:50) for 20 min protected from light, followed by two washes with 10 ml FACS buffer. Anti-CYP2E1 antibody (Thermofisher #PA5-35351) was conjugated with allophycocyanin (APC) (Expedeon # SKU705-0030), following the instructions. After the final wash, the cell pellet was resuspended in FACS buffer to a concentration of 1X106 cells/ml. Samples were loaded onto a Sony SH800 cell sorter (100 µm chip), and the target populations were gated as showed in Extended data Fig. 9a. Target populations were collected with culture medium, then seeded in a 96 well seahorse culture plate with co-culture inserts for functional analysis (see description of co-culture experiments, methods). Extracellular respiration experiment was performed after 4 days of co-culture.
Instrument	MoFlo Astrios EQ Cell Sorter ; Sony SH800 cell sorter
Software	FlowJo 10.4.2

Cell population abundance	The purity of the sorted nuclei were confirmed by single nucleus RNAseq and qPCR.
Gating strategy	For Fig. 1a, the gating strategy is: Hoechst/ tdTomato (Hoechst+ tomato+ nuclei, Hoechst++ tomato+ nuclei, Hoechst+ tomato- nuclei, Hoechst++ tomato- nuclei). For extended Fig. 9a, the gating strategy is: FSC-H/SSC-A (Adipocytes)--- UCP1:GFP/ CYP2E1:APC (CYP2E1+ adipocytes, UCP1-GFP+ adipocytes). The positive gates was made based on the staining controls showed in extended Fig. 9b. For extended Fig. 9b, in the left panel, the gating strategy is: FSC-H/SSC-A (Adipocytes)--- UCP1:GFP/ CYP2E1:APC (CYP2E1+ adipocytes, UCP1-GFP+ adipocytes). This is a staining control for gating CYP2E1+ population. In the right panel, the gating strategy is: FSC-H/SSC-A (Adipocytes)--- UCP1:GFP/ CYP2E1:APC (CYP2E1+ adipocytes, UCP1-GFP+ adipocytes). This is a staining control for gating CYP2E1+ population and UCP1-GFP+ population.

☒ Tick this box to confirm that a figure exemplifying the gating strategy is provided in the Supplementary Information.